The CD4 transmembrane GGXXG and juxtamembrane (C/F)CV+C motifs mediate pMHCII-specific signaling independently of CD4-Lck interactions

Mark S. Lee[1], Peter J. Tuohy[1], Caleb Y. Kim[1], Philip P. Yost[1], Katrina Lichauco[1], Heather L. Parrish[1], Koenraad Van Doorslaer[1, 2, 3, 4, 5, 6], and Michael S. Kuhns[1, 3, 4, 5, 6]

[1] Department of Immunobiology, The University of Arizona College of Medicine, Tucson, AZ 85724, USA.

[2] School of Animal and Comparative Biomedical Sciences, The University of Arizona, Tucson, AZ 85724, USA.

[3] Cancer Biology Graduate Interdisciplinary Program and Genetics Graduate Interdisciplinary Program, The University of Arizona, Tucson, AZ 85724, USA.

[4] The BIO-5 Institute, The University of Arizona, Tucson, AZ 85724, USA.

[5] The University of Arizona Cancer Center, Tucson, AZ, USA

[6] The Arizona Center on Aging, The University of Arizona College of Medicine, Tucson, AZ, USA

[*]Correspondence: vandoorslaer@arizona.edu, mkuhns@email.arizona.edu

Running title: The CD4 GGXXG and (C/F)CV+C motifs are key determinants of pMHCII-specific signaling.

Abstract

$CD4^+$ T cell activation is driven by 5-module receptor complexes. The T cell receptor (TCR) is the receptor module that binds composite surfaces of peptide antigens embedded within MHCII molecules (pMHCII). It associates with three signaling modules (CD3γε, CD3δε, and CD3ζζ) to form TCR-CD3 complexes. CD4 is the coreceptor module. It reciprocally associates with TCR-CD3-pMHCII assemblies on the outside of a $CD4^+$ T cells and with the Src kinase, Lck, on the inside. Previously, we reported that the CD4 transmembrane GGXXG motif and cytoplasmic juxtamembrane (C/F)CV+C motif found in eutherian CD4 (placental mammals) have constituent residues that evolved under purifying selection. Mutating these motifs together increased CD4-Lck association but reduced CD3ζ, Zap70, and Plcγ1 phosphorylation levels, as well as IL-2 production, in response to agonist pMHCII. Because these mutants preferentially localized CD4-Lck pairs to non-raft membrane fractions, one explanation for our results was that they impaired proximal signaling by sequestering Lck away from TCR-CD3. An alternative hypothesis is that the mutations directly impacted signaling because the motifs normally play a Lck-independent role in signaling. The goal of this study was to discriminate between these possibilities. Our results indicate that: intracellular CD4-Lck interactions are not necessary for pMHCII-specific signal initiation; the GGXXG and (C/F)CV+C motifs are key determinants of CD4-mediated pMHCII-specific signal amplification; the GGXXG and (C/F)CV+C motifs exert their functions independently of direct CD4-Lck association. These data provide a mechanistic explanation for why residues within these motifs are under purifying selection, and thus functionally important for $CD4^+$ T cells in vivo. The results are also important to consider for biomimetic engineering of synthetic receptors.

57 **Introduction**

58 Delineating the mechanistic principles by which multi-module receptors drive complex
59 biological processes is important both for our broad understanding of receptor biology,
60 and for guiding biomimetic engineering of synthetic receptors for therapeutic purposes.
61 For example, comparing the conventional chimeric antigen receptor (CAR) framework
62 utilized in CAR-T cell therapy, which was informed by an early 1990's understanding of
63 receptor biology, with the multi-module receptors that naturally drive T cell responses
64 suggests that conventional CARs integrate with the T cell intracellular signaling
65 machinery differently than their natural counterparts (Harris and Kranz, 2016; Wu et al.,
66 2020). These differences are likely to underlie differences in signaling output, leading us
67 to posit that fully coopting T cell functions with synthetic receptors requires that they be
68 designed to integrate with the T cell's intracellular signaling machinery in a way that
69 mimics the native receptors (Kobayashi et al., 2020). Achieving this goal requires a
70 more complete understanding of the multi-module pMHC-specific receptors that
71 mediate antigen-specific T cell activation. Understanding how $CD4^+$ T cells respond is
72 particularly important for informing biomimetic engineering of CARs given recent data
73 showing that redirecting $CD4^+$ T cells with CARs is important for long-lived therapeutic
74 efficacy (Melenhorst et al., 2022).

75 $CD4^+$ T cells are driven by 5-module receptors that recognize and drive
76 responses to peptide antigens embedded within MHCII (pMHCII). Each naïve $CD4^+$ T
77 cell expresses a clonotypic receptor module, called the T cell receptor (TCR), that binds
78 specifically to unique features of composite pMHCII surfaces (Kuhns and Badgandi,
79 2012; Kuhns and Davis, 2012). The TCR lacks intracellular signaling domains and

80 instead assembles with three signaling modules (CD3γε, δε, and ζζ) that have
81 immunoreceptor tyrosine-based activation motifs (ITAMs), and other motifs, to connect
82 TCR-pMHCII interactions to the intracellular signaling apparatus. CD4 is the coreceptor
83 module. It binds pMHCII in a reciprocal fashion with TCR-CD3 on the outside of $CD4^+$ T
84 cells and interacts with the Src kinase, Lck, via an intracellular CQC zinc clasp motif and
85 helix (Huse et al., 1998; Kim et al., 2003). According to the widely accepted TCR
86 signaling paradigm, co-engagement of pMHCII by TCR-CD3 and CD4 positions Lck and
87 the CD3 ITAMs in the proper spatial proximity to enable Lck phosphorylation of the CD3
88 ITAMs to initiate signaling (Rudd, 2021). However, when we tested this model directly,
89 we found that CD4-Lck interactions are not key determinants of CD3ζ ITAM
90 phosphorylation (pCD3ζ)(Lee et al., 2022). Based on our work, as well as work from
91 other labs, we consider the question of how intracellular pMHCII-specific $CD4^+$ T cell
92 signaling is initiated to be unresolved (Glassman et al., 2018; Horkova et al., 2023;
93 Killeen and Littman, 1993; Xu and Littman, 1993).
94 The answer to this question lies with how the 5 modules of pMHCII receptors
95 evolved over 435 million years to refine pMHCII-specific signaling. In our recent
96 publication, we computationally reconstructed CD4 evolution to identify residues and
97 motifs in the extracellular, transmembrane, and intracellular domains that are of
98 functional importance (Lee et al., 2022). We then performed structure function analysis
99 with mutants of key motifs to infer their function by evaluating the phenotypes of the
100 mutants. When we mutated the intracellular CQC clasp and IKRLL helix motifs that are
101 known to mediate CD4-Lck interactions, we observed significant reductions in CD4-Lck
102 association; yet we did not observe the expected impact on CD3ζ ITAM phosphorylation

103 (pCD3ζ) predicted by the TCR signaling paradigm. In contrast, when we mutated the
104 transmembrane GGXXG motif and cytoplasmic juxtamembrane (C/F)CV+C
105 palmitoylation motif, we observed an increased frequency of CD4-Lck pairs that were
106 preferentially localized to detergent soluble membrane domains. We also found
107 evidence of reduced CD3ζ, Zap70, and Plcγ1 phosphorylation (pCD3ζ, pZap70, and
108 pPlcγ1) compared with WT CD4. The reason that constituent residues of these motifs
109 evolved under purifying selection appears to be due to reduced signaling in response to
110 pMHCII when the motifs are altered. We took these data as evidence that the GGXXG
111 and (C/F)CV+C motifs arose in eutherians (placental mammals) to tightly regulate
112 pMHCII-specific signal initiation and postulated that the mutant CD4 molecules might
113 sequester Lck away from TCR-CD3 to prevent CD3ζ phosphorylation. However, an
114 alternative hypothesis is that the GGXXG and (C/F)CV+C motifs impact pCD3ζ levels
115 independently of CD4-Lck interactions.

116 Here we took a reductionist approach to test these hypotheses by studying the
117 impact of GGXXG and (C/F)CV+C motif mutants individually, or together, on proximal
118 pMHCII-specific signaling in C-terminally truncated CD4 molecules (T1). Working with
119 T1 eliminated motifs in the intracellular domain, including those that mediate CD4-Lck
120 association. As expected from prior work, truncating CD4 relieved CD4-Lck interactions
121 yet only slightly reduced IL-2 production (Lee et al., 2022). Importantly, there was no
122 impact on average pCD3ζ levels or percent of cells with phosphorylated CD3ζ, when
123 compared with wild-type (WT) CD4, despite significantly reduced levels of CD4-Lck
124 pairs. These data provide further evidence that the core tenet of the TCR signaling
125 paradigm, wherein CD4 recruits Lck to CD3 ITAMs initiates signaling, needs revising.

126 Importantly, T1 molecules bearing mutations in the GGXXG and (C/F)CV+C motifs
127 individually or together reduced IL-2 production as well as pCD3ζ levels and other TCR-
128 proximal signaling events. The simplest interpretation of these data is that the GGXXG
129 and (C/F)CV+C motifs are key determinants of pMHCII-specific signaling on their own,
130 independent of CD4-Lck interactions.
131
132 **Results**
133 The goal of this study was to evaluate if the transmembrane GGXXG and
134 juxtamembrane palmitoylation ((C/F)CV+C) motifs influence pMHCII-specific proximal
135 signaling on their own rather than by sequestering CD4-Lck pairs away from membrane
136 rafts (**Figure 1**). Accordingly, we used 58$\alpha^-\beta^-$ T cell hybridomas transduced to express
137 the 5c.c7 TCR along with either the WT or mutant CD4 constructs described in **Table 1**.
138 The well-characterized 5c.c7 TCR recognizes the moth cytochrome c peptide 88-103
139 (MCC) in the context of mouse MHCII I-E^k. We used this experimental system because
140 58$\alpha^-\beta^-$ cells were used in seminal work that helped form the foundation of the TCR
141 signaling paradigm (Glaichenhaus et al., 1991). In that study, a loss of CD4-Lck
142 interactions due to mutating the intracellular CQC clasp motif was linked with reduced
143 signaling output as measured by IL-2 production. Furthermore, IL-2 production by these
144 58$\alpha^-\beta^-$ cells is CD4 dependent, indicating that relevant signaling pathways are intact.
145
146 **WT and T1 equivalently enhance pMHCII-specific proximal signaling.** We
147 previously reported that the C-terminally truncated mouse CD4-T1 mutant (**T1: Table 1**
148 **and Figure 1 arrow**) had only a minor impact on IL-2 production relative to WT CD4

149 despite lacking most of the intracellular domain, including the CQC clasp and IKRLL
150 motifs shown to mediate CD4-Lck association (Lee et al., 2022). Because T1 maintains
151 both the transmembrane GGXXG and juxtamembrane (C/F)CV+C motifs, we reasoned
152 that it had utility for studying the contributions these motifs make to pMHCII-specific
153 signaling in the absence of CD4-Lck interactions.

154 Accordingly, we generated 5c.c7^{+} 58$\alpha^{-}\beta^{-}$ cells expressing WT CD4, T1, or T1
155 combined with our previously reported Δbind mutant, which disrupts binding to pMHCII
156 in the CD4 D1 domain as well as signaling output (**Table 1 and Figure 2 – figure**
157 **supplement 1**)(Glassman et al., 2016; Glassman et al., 2018; Parrish et al., 2015). The
158 goals were to determine: 1) if T1 significantly impairs pMHCII-specific proximal signaling
159 events, relative to WT, as expected based on the TCR signaling paradigm because it
160 lacks the CQC and IKRLL motifs that mediate CD4-Lck interactions; 2) use T1$^{\Delta bind}$ to
161 determine the overall contribution of pMHCII-dependent assembly of CD4 with TCR-
162 CD3 to proximal signaling. For IL-2 production, we observed a slightly reduced
163 magnitude of the response that was consistent across a range of MCC peptide
164 concentrations for T1 compared to WT (**Figure 2A**). We also observed reduced
165 pMHCII-specific endocytosis for T1 compared to WT (**Figure 2 – figure supplement 2)**.
166 Importantly, the T1$^{\Delta bind}$ mutant did not produce IL-2 or undergo pMHCII-specific
167 endocytosis. These data indicate that, in our system, extracellular CD4-pMHCII
168 engagement is critical for IL-2 production while the CD4 intracellular domain C-terminal
169 of R422 can be deleted.

170 Next, we evaluated the impact of these mutations on proximal signaling events
171 measured by flow cytometry in response to antigen presenting cells (APCs) expressing

172 agonist MCC:I-E^k after background subtraction of signal levels in response to APCs
173 expressing null Hb:I-E^k (**Figure 2 – figure supplement 3**). Our analysis of five
174 independently generated pairs of WT and T1 cell lines showed variable difference in
175 pCD3ζ levels. For three pairs of lines, the T1 response was higher than the WT and for
176 two it was lower (**Figure 2B**). The averages of the T1 response normalized to the paired
177 WT controls showed no difference between the population. There were also no
178 differences for the average percent of T1 cells with response levels to MCC that were
179 above the null Hb peptide when normalized to their paired WT controls. Similar results
180 were observed for pZap70 and pPlcγ1 levels (**Figure 2 – figure supplement 4**). These
181 data, summarized in **Table 2,** provide additional evidence that CD4-Lck interactions via
182 the CQC clasp and IKRLL motifs are not key determinants of pMHCII-specific early
183 signal events or IL-2 production in this experimental system.
184 In contrast, the $T1^{\Delta bind}$ mutant significantly reduced pCD3ζ, pZap70, or pPlcγ1
185 levels compared to the T1 control but did not obviously impact the percent of cells
186 responding to agonist MCC:I-E^k (**Figure 2C and Figure 2 – figure supplement 5**).
187 Because the antibodies used to detect pCD3ζ, pZap70, and pPlcγ1 recognize single
188 phosphorylated tyrosines, these data indicate that CD4 enhances the number of TCR-
189 CD3 complexes per cell with phosphorylated CD3ζ molecules at Y142 (same in human
190 and mouse), as well as the number of phosphorylated Zap70 and Plcγ1 molecules per
191 cell, in a manner that is dependent on TCR-CD3 and CD4 co-engagement of pMHCII
192 but independent of the intracellular domain C-terminal of R422. A summary of these
193 results can be found in **Table 3**.
194

195 **The GGXXG and (C/F)CV+C motifs influence IL-2 production independently of**
196 **Lck.**
197 Having established that T1 contributes to early pMHCII-specific signaling (e.g. pCD3ζ)
198 as well as signaling output (i.e. IL-2), we generated 5c.c7^{+} 58$\alpha^{-}\beta^{-}$ cells expressing WT,
199 T1, or the truncated T1 wherein the GGXXG and/or (C/F)CV+C motifs are also mutated
200 (**Table 1 and Figure 3 – figure supplement 1**). To study the function of the GGXXG
201 motif alone, we used our previously described TMD mutant (GGXXG to GVXXL)
202 wherein bulky side chains replace the glycines that compose a flat surface on the
203 transmembrane helix that could mediate protein:protein or protein:cholesterol
204 interactions (Fessler, 2016; Parrish et al., 2015; Song et al., 2014; Teese and
205 Langosch, 2015; Wacker et al., 2013). We called these mutants T1-TMD. To test the
206 function of the palmitoylation motif, which contains the core CVRC (418-421) sequence
207 in mouse and humans, we made note of a broader (C/F)CVRC motif in eutherians
208 wherein the majority of ortholog sequences had CCVRC, as found in mouse, and a
209 minority had FCVRC as found in humans. Importantly, we previously noted that position
210 417 is under purifying selection for all extant CD4 orthologs we analyzed by the fixed
211 effects likelihood (FEL) method, indicating that this residue evolved under purifying
212 selection due to functional importance (Lee et al., 2022). We therefore made T1-Palm
213 (3C) mutants wherein we mutated all three cysteines to serines as well as T1-Palm (2C)
214 mutants where only the core cysteines common to mouse and humans were mutated to
215 serines, as in our prior analysis of CD4 WT. Finally, we made mutants containing both
216 the TMD and Palm mutants that we called T1-TP(3C) or T1-TP(2C).
217 To confirm that truncating CD4 relieved CD4-Lck association, and evaluate if the

218 mutations impacted any residual CD4-Lck interactions that may occur due to
219 colocalization in particular membrane domains, we performed sucrose gradient analysis
220 of detergent lysates of WT, T1, T1-TMD, T1-Palm(2C), T1-Palm(3C), T1-TP(2C) and
221 T1-TP(3C). We observed significantly reduced CD4-Lck association in detergent
222 resistant membranes (DRMs, aka membrane rafts) and detergent soluble membranes
223 (DSMs) for T1 compared to WT (**Figure 3 – figure supplement 2**)(Pike, 2006). The
224 mutants did not impact residual CD4-Lck association in the DRMs or DSMs.
225 Furthermore, the total Lck signal associated with CD4 was significantly lower for T1
226 compared with the WT, and the residual association was not impacted by the mutants
227 (**Table 3 and Figure 3 – figure supplement 3**). We therefore conclude that, in our
228 experimental system, any functional differences between the T1-TMD, T1-Palm(2C/3C),
229 or T1-TP(2C/3C) mutants and the T1 control is a function of the motif we are studying in
230 the absence of direct CD4-Lck interactions.
231 Next, we measured IL-2 production by WT, T1, and CD4 mutant cells to evaluate
232 the impact of the mutations on signaling output in response to MCC. Here again, T1
233 was slightly lower than WT, while the T1-TMD reduced the IL-2 response magnitude
234 and sensitivity relative to the T1 control (**Figure 3A**). This was expected given our prior
235 work showing that the TMD mutant reduced IL-2 production driven by a shorter CD4
236 truncation mutant (CD4T, mutated at R420)(Parrish et al., 2015). Mutating the GGXXG
237 or (C/F)CV+C motifs individually or together did not impact pMHCII-induced TCR
238 endocytosis relative to the T1 control, and activation-induced CD4 endocytosis was
239 inhibited for all truncated CD4 molecules (**Figure 3 – figure supplement 4A and 4B**).
240 The T1-Palm(2C), T1-TP(2C), T1-Palm(3C), and T1-TP(3C) all reduced IL-2 production

241 relative to T1, indicating that they also influence the Lck-independent contribution of
242 CD4 to pMHCII-specific signaling (**Figure 3B**). Of note, the T1-TP(2C) IL-2 response
243 magnitude was lower than that of T1-Palm(2C) alone, consistent with what we
244 previously observed with the full-length versions of these CD4 mutants (**Figure 3B**)(Lee
245 et al., 2022). Furthermore, the T1-Palm(3C) response magnitude was lower than that of
246 T1-Palm(2C), suggesting that the additional cysteine contributes to signaling. Together,
247 these data indicate that the GGXXG and (C/F)CV+C motifs contribute to the signaling
248 cascade that leads to pMHCII-specific IL-2 production when CD4 does not directly
249 interact with Lck via the intracellular CQC clasp and IKRLL motifs. These data do not
250 tell us where in the signaling pathway the contributions are made.
251
252 **The CD4 GGXXG and (C/F)CV+C motifs are key determinants of proximal**
253 **signaling.**
254 To evaluate if the GGXXG and (C/F)CV+C motifs influence early signaling events, we
255 measured pCD3ζ, pZap70, and pPlcγ1 levels for four independently generated T1-TMD
256 lines, three independently generated T1-Palm(2C) lines, and three independently
257 generated T1-TP(2C) lines relative to their matched T1 controls in response to APCs
258 expressing MCC:I-E^k, as introduced above (**Figure 2 – figure supplement 3**). For each
259 T1-TMD and T1-TP(2C) mutant line, we observed lower pCD3ζ, pZap70, and pPlcγ1
260 levels than their paired T1 control. For the T1-Palm(2C) lines, all 3 showed reduced
261 pCD3ζ levels, but only 2 of 3 showed reduced pZap70, and pPlcγ1 levels (**Figure 4A**
262 **and Figure 4 – Figure supplement 1A and 2A**). These data indicate that the GGXXG
263 and (C/F)CV+C motifs contribute to CD4's ability to enhance proximal signaling in the

264 absence of CD4-Lck interactions.

265 We also considered the average fold change of the means of the independently
266 generated mutant cell lines relative to their paired T1 controls (**Figure 4B and Figure 4**
267 **– Figure supplement 1B and 2B**). For this analysis we included the mean of the fold
268 change of the T1$^{\Delta bind}$ mutant cells from Figure 2C relative to their paired T1 controls
269 (dotted line) as a visual to consider the severity of the impact of the mutations on
270 proximal signaling relative to the contributions of T1, which can bind pMHCII, as well as
271 the level of signaling observed with T1$^{\Delta bind}$ that cannot bind pMHCII. The T1-TMD and
272 T1-Palm(2C) showed reduced pCD3ζ and pZap70 levels midway between T1 and
273 T1$^{\Delta bind}$, while the T1-TP(2C) mutant closely approximated the dotted line representing
274 the signaling observed in the T1$^{\Delta bind}$ cells. Differences in the average pPlcγ1 responses
275 were less pronounced. These data further suggest a role for the GGXXG and
276 (C/F)CV+C motifs in contributing to CD4-mediated pMHCII-specific signaling in the
277 absence of CD4-Lck interactions.

278 Because we had found that T1$^{\Delta bind}$ cells failed to produce IL-2 in response to high
279 peptide concentrations in our dose response experiments (**Figure 1A**), whereas the T1-
280 TP(2C) mutant cells made IL-2 in response to high peptide concentrations (**Figure 3B**),
281 we found it interesting that the early signaling responses we measure to APCs
282 expressing high ligand densities of tethered pMHCII were similar between the T1$^{\Delta bind}$
283 and T1-TP(2C) cells. We therefore evaluated IL-2 production of the T1, T1$^{\Delta bind}$, and T1-
284 TP(2C) in response to the APCs used in these signaling studies to ask if they followed
285 the same pattern of responses to high peptide doses in our prior experiments. As
286 expected, we found that the T1-TP(2C) cells made approximately half as much IL-2 as

287 the T1 controls, whereas IL-2 production by the T1$^{\Delta bind}$ cells was negligible (**Figure 4 –**
288 **Figure supplement 3**). These data indicate that the ability of CD4 to interact with
289 pMHCII can partially overcome the loss of function of the GGXXG and (C/F)CV+C
290 motifs at high ligand densities with respect to a downstream signaling output, such as
291 IL-2 production, even if the early signaling events measured at 2 minutes after pMHCII-
292 engagement were similar.

293 Finally, we considered the percent of mutant responders normalized to the
294 controls. We observed small decreases in T1-TP(2C) cells with pCD3ζ and pZap70
295 levels relative to the control, while pPlcγ1 trended lower for this mutant. The single
296 mutants were roughly equivalent to their matched T1 controls. These data indicate that
297 mutating the GGXXG and (C/F)CV+C motifs together in the absence of the intracellular
298 domain can reduce the number of cells that initiate pMHCII-specific signaling (**Figure**
299 **4C and Figure 4 – Figure supplement 1C and 2C**). We did not observe this
300 phenotype in our prior study when the intracellular domain was present, suggesting this
301 is unique to the absence of the intracellular domain.

302 We also measured early signaling for three independently generated T1-
303 Palm(3C) and T1-TP(3C) mutant cell lines compared to their paired T1 controls. For all
304 lines, pCD3ζ, pZap70, and pPlcγ1 levels were significantly lower than the controls,
305 which was reflected in the normalized fold change (**Figure 5A and 5B and Figure 5 –**
306 **figures supplement 1A, 1B, 2A, 2B**). The fold change for the T1-TP(3C) levels relative
307 to the controls was similar to the T1$^{\Delta bind}$ cells (**Figure 5B and Figure 5 – figures**
308 **supplement 1B and 2B**). These data provide further evidence that the GGXXG and
309 (C/F)CV+C motifs together are key determinants of the Lck-independent contributions

310 that CD4 makes to amplifying pMHCII-specific proximal signaling.

311 Finally, the percent responders were only lower for pZap70 for both T1-Palm(3C)
312 and T1-TP(3C) relative to WT, while pCD3ζ and pPlcγ1 trended lower (**Figure 5 and**
313 **Figure 5 – figures supplement 1C and 2C**). These data are consistent with the idea
314 that, in the absence of the intracellular domain, mutating these motifs influences
315 initiation of key signaling events. See **Table 3** for a summary of the data.

316

317 **Discussion**

318 Our computational reconstruction of CD4 evolution provided access to a subset of
319 results from experiments that Nature performed over ~435 million years in a greater
320 variety of jawed vertebrates than could be achieved with mouse or human studies (Lee
321 et al., 2022). It allowed us to identify residues that were selected under purifying
322 selection, and thus functionally significant, because acquiring a mutation at these
323 residues affects fitness and results in a failure to propagate the change to future
324 progeny. Our structure-function analysis of these residues in $58\alpha^{-}\beta^{-}$ cells, which we
325 continued in this study, has started to provide mechanistic insights into why these
326 residues are functionally important.

327 The data presented here are inconsistent with the prevailing model in which CD4
328 recruits Lck to CD3 ITAMs to initiate signaling. The decrease in pMHCII-specific IL-2
329 production when the CD4 intracellular domain is truncated cannot be attributed to
330 reductions in early signaling events such as pCD3ζ. Importantly, the pCD3ζ levels were
331 ~2 fold lower in the absence of CD4-pMHCII interactions ($T1^{\Delta bind}$ mutant) under the
332 experimental conditions tested here. We take these data as evidence that there is a

333 threshold for the number of CD3ζ molecules phosphorylated, and/or the duration of
334 signaling, that is required to drive IL-2 production in our system. We also conclude that
335 CD4 binding to pMHCII functions to increase the number of TCR-CD3 complexes per
336 cell that experience CD3ζ phosphorylation to reach that threshold and/or sustain
337 signaling and that it similarly impacts pZap70 levels as well as pPlcγ1 levels, albeit to a
338 lesser extent for the latter.

339 A logical extension of these conclusions is that there is a density of agonist
340 pMHCII below which CD4 binding to pMHCII is essential for signal initiation. This idea is
341 supported by findings that CD4 is necessary for signal propagation and amplification to
342 the calcium mobilization step in response to fewer than 25 agonist pMHCII (Irvine et al.,
343 2002). Attempting to accurately measure the contributions of CD4 to ITAM
344 phosphorylation, with or without mutant motifs, at very low densities of pMHCII would be
345 challenging and is technically beyond the scope of this study. Nevertheless, in this and
346 our prior study we did not observe the expected decreases in pCD3ζ levels when CD4-
347 Lck interactions were reduced by mutating the CQC clasp motif, the IKRLL motif, or by
348 eliminating the intracellular domain. Furthermore, we found in our prior study that IL-2
349 production increased significantly when we mutated the full intracellular helix, the helix
350 and CQC clasp together, or the IKRLL motif alone. These direct tests of the TCR
351 signaling paradigm are inconsistent with predictions of the model. As such, they suggest
352 the contributions of CD4 to signal initiation and amplification at the early timepoint we
353 measured are independent of direct CD4-Lck interactions.

354 Because the combined impact of mutating the GGXXG and (C/F)CV+C motifs on
355 pCD3ζ levels were roughly equivalent to disrupting CD4-pMHCII engagement, even

356 when direct CD4-Lck interactions were absent, we can conclude that the GGXXG and
357 (C/F)CV+C motifs are key determinants that help CD4 drive signaling above the
358 threshold required for IL-2 production. Our data also provide evidence that mutating the
359 GGXXG and (C/F)CV+C motifs together can reduce the frequency of cells experiencing
360 CD3ζ and Zap70 phosphorylation in the absence of the intracellular domain. Given that
361 palmitoylation is rapidly reversable, these data suggest that the switch-like function of
362 the palmitoylation motif may influence signal initiation. Interestingly, unlike CD4-pMHCII
363 interactions, these motifs are not essential for signaling output at high ligand densities
364 as we observed low levels of IL-2 produced in cells bearing mutants of these motifs with
365 increasing doses of agonist pMHCII. Reciprocal binding of CD4 and TCR-CD3 to
366 pMHCII can therefore amplify pMHCII-specific signaling without the contributions of the
367 GGXXG and (C/F)CV+C motifs, or motifs in the intracellular domain, albeit at lower
368 levels than if these motifs are intact. This could be due to the contributions of additional
369 unidentified motifs in the transmembrane domain, or to the increase in TCR-CD3 dwell
370 time on pMHCII that is mediated by the CD4 extracellular domain (Glassman et al.,
371 2018). Given that these motifs were essential for IL-2 production at low ligand densities,
372 a logical extension of these data is that there is an agonist pMHCII density below which
373 these motifs are essential for the initiation of early signaling events.
374 The data from our current study indicate that the GGXXG and (C/F)CV+C motifs
375 do not influence early signaling events by regulating the ability of CD4 to either recruit
376 Lck to, or sequester it away from, the TCR-CD3 ITAMs as we previously postulated
377 (Lee et al., 2022). Instead, they work independently of CD4-Lck interactions to enhance
378 pMHCII-specific signaling. It is tempting to speculate that because these motifs can

379 regulate CD4 membrane domain localization and, in other proteins, palmitate moieties
380 can sandwich cholesterol against the flat surface of a GG patch on a transmembrane
381 domain helix, these motifs may allow CD4 to regulate local concentration of cholesterol
382 or cholesterol sulfate around TCR-CD3, perhaps by taking such molecules away from
383 TCR-CD3 to stabilize allosteric changes associated with signaling (Chen et al., 2022;
384 Fessler, 2016; Gil et al., 2002; Lee et al., 2015; Song et al., 2014; Swamy et al., 2016;
385 Teese and Langosch, 2015; Wacker et al., 2013; Wang et al., 2016). These CD4 motifs
386 may also impact the accessibility of ITAMs for Lck phosphorylation by changing the
387 local membrane environment around TCR-CD3 upon reciprocal engagement of pMHCII
388 (Aivazian and Stern, 2000; Xu et al., 2008). Finally, it is worth considering that, in our
389 prior study, we found G402 of the GGXXG motif has covaried over evolutionary time
390 with L438 of the intracellular helix IKRLL motif that has inhibitory function, suggesting
391 that the function of these motifs are co-evolving (Lee et al., 2022). In support of this
392 idea, we reported in that study that the signal enhancing activity of the GGXXG and
393 (C/F)CV+C motifs together counterbalanced the inhibitory activity of the IKRLL motif
394 with regards to IL-2 production. It is unclear at this point if this counterbalancing is
395 simply additive of individual motif functions, or if there is a functional interplay of the
396 motifs when the intracellular domain of CD4 is present. Delineating the mechanistic
397 details by which the GGXXG and (C/F)CV+C motifs increase signaling on their own, or
398 when combined, and how their function integrates with those of other motifs will be the
399 subject of future investigations.

400 Altogether, the data in this and our preceding study provide direct evidence that
401 complement indirect results indicating that pMHCII-specific signaling is not initiated, or

402 dependent on, CD4 recruitment of Lck to the CD3 ITAMs (Glassman et al., 2018;
403 Horkova et al., 2023; Killeen and Littman, 1993; Lee et al., 2022; Xu and Littman, 1993).
404 Recent work on CD8 suggest that this coreceptor also does not recruit Lck to
405 phosphorylate CD3 ITAMs (Casas et al., 2014; Wei et al., 2020). In total, these findings
406 suggest that the TCR signaling paradigm needs revising as it pertains to coreceptor-Lck
407 interactions. For CD4, the existing evidence suggest that reciprocal binding of CD4 and
408 TCR-CD3 enables free Lck and Fyn to initiate signaling by phosphorylating the ITAMs
409 and Zap70 (Glassman et al., 2016; Glassman et al., 2018; Horkova et al., 2023; Lee et
410 al., 2022; Salmond et al., 2009; van Oers et al., 1996). The contribution of the current
411 study is in showing the GGXXG and (C/F)CV+C motifs work together to enhance these
412 early signaling events independently of direct CD4-Lck interactions.
413 It is interesting to consider what the primary purpose of CD4-Lck interactions via
414 the CQC clasp and IKRLL motifs are if not to recruit Lck to the CD3 ITAMs. Data from
415 two studies suggest that Lck makes a kinase-independent contribution to pMHCII-
416 specific responses; it is therefore plausible that the phenotype reported for CD4 when
417 the CQC clasp is mutated is due to relieving the kinase-independent scaffolding function
418 of Lck (Horkova et al., 2023; Xu and Littman, 1993). In addition, CD4-Lck interaction via
419 the CQC clasp motif and the intracellular helix will prevent the helix from interacting with
420 other partners, thus mutating the CQC clasp would favor helix interactions with other
421 putative partners (Lee et al., 2022). Finally, the CQC clasp is thought to play a role in
422 positioning CD4 in proximity to Lat, either through direct or indirect interactions, which
423 could contribute to the phenotype of CQC clasp mutants (Bosselut et al., 1999; Lo et al.,
424 2018; Lo et al., 2019). If CD4-Lck and CD4-Lat interactions are mutually exclusive, and

425 both require the CQC clasp, then mutating this motif would have a greater impact than
426 just relieving CD4-Lck interactions (Bosselut et al., 1999). These questions remain
427 outstanding, as do questions concerning how the intracellular helix regulates pMHCII-
428 specific signaling.

429 The broader implications of the data presented in our current and prior evolution-
430 structure-function studies provide fertile ground for future directions beyond those
431 mentioned above. Our approach allows us to identify functionally important
432 residues/motif and then interrogate basic principles of their function that should hold
433 true across $CD4^+$ T cell subsets since the biochemical and biophysical bases for
434 interactions between CD4 and its interacting partners (i.e. other proteins or membrane
435 components) should be the same in $58\alpha^-\beta^-$ cells as in thymocytes or in different $CD4^+$ T
436 cells. However, different $CD4^+$ T cell populations will have different levels of expression
437 of relevant proteins (e.g. interacting partners or modifying enzymes), and may even
438 have differences in lipid composition, such that the impact of the motifs we have
439 identified and studied to date may lead to different outcomes in different $CD4^+$ T cell
440 subsets (http://immpres.co.uk/)(Tuosto and Xu, 2018). For example, differences in
441 expression of enzymes with switch-like functions, such as those that add or remove
442 palmitate to the (C/F)CV+C motif, or those that phosphorylate or dephosphorylate the
443 serines in the intracellular helix that regulate CD4-Lck interactions and inhibitory activity,
444 may vary between naïve $CD4^+$ T cells, different Th subsets, or Tregs to differentially
445 tune the activity of these motifs and their impact on pMHCII-specific signaling. Now that
446 we have identified residues and broader motifs that have proven to be functionally
447 important *in vivo* over 435 million years of evolution, while also providing mechanistic

448 insights as to why the residues are important, there is utility in evaluating the impact of
449 mutant CD4 conditional knock-in mice on thymocyte development, naïve $CD4^+$ T cell
450 activation and differentiation, and the execution of Th and Treg effector functions. In so
451 doing, we will gain additional insights into why there is a fitness cost if a mutation is
452 acquired in these residues. Such knowledge will increase our fundamental
453 understanding of $CD4^+$ T cell biology and will also be critical for biomimetic engineering
454 of synthetic receptors that can redirect $CD4^+$ T cell activity for therapeutic purposes.
455

456 **Materials and methods**

457 The work performed in this manuscript was conducted according to the materials and
458 methods of our previous study, which can be found here:
459 https://elifesciences.org/articles/79508#s4.
460

461 **Funding**

462 This work was supported by R01AI101053 (MSK), CCSG-CA 023074 (MSK), and AZ
463 TRIF funds (KVD).

464 **References**
465

466 Aivazian, D., and Stern, L.J. (2000). Phosphorylation of T cell receptor zeta is regulated
467 by a lipid dependent folding transition. Nat Struct Biol *7*, 1023-1026.

468 Bosselut, R., Zhang, W., Ashe, J.M., Kopacz, J.L., Samelson, L.E., and Singer, A.
469 (1999). Association of the adaptor molecule LAT with CD4 and CD8 coreceptors
470 identifies a new coreceptor function in T cell receptor signal transduction. J Exp Med
471 *190*, 1517-1526.

472 Casas, J., Brzostek, J., Zarnitsyna, V.I., Hong, J.S., Wei, Q., Hoerter, J.A., Fu, G.,
473 Ampudia, J., Zamoyska, R., Zhu, C., and Gascoigne, N.R. (2014). Ligand-engaged TCR
474 is triggered by Lck not associated with CD8 coreceptor. Nat Commun *5*, 5624.

475 Chen, Y., Zhu, Y., Li, X., Gao, W., Zhen, Z., Dong, Huang, B., Ma, Z., Zhang, A., Song,
476 X.*, et al.* (2022). Cholesterol inhibits TCR signaling by directly restricting TCR-CD3 core
477 tunnel motility. Mol Cell.

478 Fessler, M.B. (2016). The Intracellular Cholesterol Landscape: Dynamic Integrator of
479 the Immune Response. Trends Immunol *37*, 819-830.

480 Gil, D., Schamel, W.W., Montoya, M., Sanchez-Madrid, F., and Alarcon, B. (2002).
481 Recruitment of Nck by CD3 epsilon reveals a ligand-induced conformational change
482 essential for T cell receptor signaling and synapse formation. Cell *109*, 901-912.

483 Glaichenhaus, N., Shastri, N., Littman, D.R., and Turner, J.M. (1991). Requirement for
484 association of p56lck with CD4 in antigen-specific signal transduction in T cells. Cell *64*,
485 511-520.

486 Glassman, C.R., Parrish, H.L., Deshpande, N.R., and Kuhns, M.S. (2016). The CD4
487 and CD3deltaepsilon Cytosolic Juxtamembrane Regions Are Proximal within a Compact
488 TCR-CD3-pMHC-CD4 Macrocomplex. J Immunol *196*, 4713-4722.

489 Glassman, C.R., Parrish, H.L., Lee, M.S., and Kuhns, M.S. (2018). Reciprocal TCR-
490 CD3 and CD4 Engagement of a Nucleating pMHCII Stabilizes a Functional Receptor
491 Macrocomplex. Cell Rep *22*, 1263-1275.

492 Harris, D.T., and Kranz, D.M. (2016). Adoptive T Cell Therapies: A Comparison of T
493 Cell Receptors and Chimeric Antigen Receptors. Trends Pharmacol Sci *37*, 220-230.

494 Horkova, V., Drobek, A., Paprckova, D., Niederlova, V., Prasai, A., Uleri, V., Glatzova,
495 D., Kraller, M., Cesnekova, M., Janusova, S.*, et al.* (2023). Unique roles of co-receptor-
496 bound LCK in helper and cytotoxic T cells. Nat Immunol *24*, 174-185.

497 Huse, M., Eck, M.J., and Harrison, S.C. (1998). A Zn2+ ion links the cytoplasmic tail of
498 CD4 and the N-terminal region of Lck. J Biol Chem *273*, 18729-18733.

499 Irvine, D.J., Purbhoo, M.A., Krogsgaard, M., and Davis, M.M. (2002). Direct observation
500 of ligand recognition by T cells. Nature *419*, 845-849.

501 Killeen, N., and Littman, D.R. (1993). Helper T-cell development in the absence of CD4-
502 p56lck association. Nature *364*, 729-732.

503 Kim, P.W., Sun, Z.Y., Blacklow, S.C., Wagner, G., and Eck, M.J. (2003). A zinc clasp
504 structure tethers Lck to T cell coreceptors CD4 and CD8. Science *301*, 1725-1728.

505 Kobayashi, S., Thelin, M.A., Parrish, H.L., Deshpande, N.R., Lee, M.S., Karimzadeh, A.,
506 Niewczas, M.A., Serwold, T., and Kuhns, M.S. (2020). A biomimetic five-module
507 chimeric antigen receptor ((5M)CAR) designed to target and eliminate antigen-specific T
508 cells. Proc Natl Acad Sci U S A *117*, 28950-28959.

509 Kuhns, M.S., and Badgandi, H.B. (2012). Piecing together the family portrait of TCR-
510 CD3 complexes. Immunol Rev *250*, 120-143.

511 Kuhns, M.S., and Davis, M.M. (2012). TCR Signaling Emerges from the Sum of Many
512 Parts. Frontiers in immunology *3*, 159.

513 Lee, M.S., Glassman, C.R., Deshpande, N.R., Badgandi, H.B., Parrish, H.L.,
514 Uttamapinant, C., Stawski, P.S., Ting, A.Y., and Kuhns, M.S. (2015). A Mechanical
515 Switch Couples T Cell Receptor Triggering to the Cytoplasmic Juxtamembrane Regions
516 of CD3zetazeta. Immunity *43*, 227-239.

517 Lee, M.S., Tuohy, P.J., Kim, C.Y., Lichauco, K., Parrish, H.L., Van Doorslaer, K., and
518 Kuhns, M.S. (2022). Enhancing and inhibitory motifs regulate CD4 activity. eLife *11*,
519 e79508.

520 Lo, W.L., Shah, N.H., Ahsan, N., Horkova, V., Stepanek, O., Salomon, A.R., Kuriyan, J.,
521 and Weiss, A. (2018). Lck promotes Zap70-dependent LAT phosphorylation by bridging
522 Zap70 to LAT. Nat Immunol *19*, 733-741.

523 Lo, W.L., Shah, N.H., Rubin, S.A., Zhang, W., Horkova, V., Fallahee, I.R., Stepanek, O.,
524 Zon, L.I., Kuriyan, J., and Weiss, A. (2019). Slow phosphorylation of a tyrosine residue
525 in LAT optimizes T cell ligand discrimination. Nat Immunol *20*, 1481-1493.

526 Melenhorst, J.J., Chen, G.M., Wang, M., Porter, D.L., Chen, C., Collins, M.A., Gao, P.,
527 Bandyopadhyay, S., Sun, H., Zhao, Z.*, et al.* (2022). Decade-long leukaemia remissions
528 with persistence of CD4(+) CAR T cells. Nature *602*, 503-509.

529 Parrish, H.L., Glassman, C.R., Keenen, M.M., Deshpande, N.R., Bronnimann, M.P., and
530 Kuhns, M.S. (2015). A Transmembrane Domain GGxxG Motif in CD4 Contributes to Its
531 Lck-Independent Function but Does Not Mediate CD4 Dimerization. PLoS One *10*,
532 e0132333.

533 Pike, L.J. (2006). Rafts defined: a report on the Keystone Symposium on Lipid Rafts
534 and Cell Function. J Lipid Res *47*, 1597-1598.

535 Rudd, C.E. (2021). How the Discovery of the CD4/CD8-p56(lck) Complexes Changed
536 Immunology and Immunotherapy. Front Cell Dev Biol *9*, 626095.

537 Salmond, R.J., Filby, A., Qureshi, I., Caserta, S., and Zamoyska, R. (2009). T-cell
538 receptor proximal signaling via the Src-family kinases, Lck and Fyn, influences T-cell
539 activation, differentiation, and tolerance. Immunol Rev *228*, 9-22.

540 Song, Y., Kenworthy, A.K., and Sanders, C.R. (2014). Cholesterol as a co-solvent and a
541 ligand for membrane proteins. Protein Sci *23*, 1-22.

542 Swamy, M., Beck-Garcia, K., Beck-Garcia, E., Hartl, F.A., Morath, A., Yousefi, O.S.,
543 Dopfer, E.P., Molnar, E., Schulze, A.K., Blanco, R.*, et al.* (2016). A Cholesterol-Based
544 Allostery Model of T Cell Receptor Phosphorylation. Immunity *44*, 1091-1101.

545 Teese, M.G., and Langosch, D. (2015). Role of GxxxG Motifs in Transmembrane
546 Domain Interactions. Biochemistry *54*, 5125-5135.

547 Tuosto, L., and Xu, C. (2018). Editorial: Membrane Lipids in T Cell Functions. Frontiers
548 in immunology *9*, 1608.

549 van Oers, N.S., Lowin-Kropf, B., Finlay, D., Connolly, K., and Weiss, A. (1996). alpha
550 beta T cell development is abolished in mice lacking both Lck and Fyn protein tyrosine
551 kinases. Immunity *5*, 429-436.

552 Wacker, D., Wang, C., Katritch, V., Han, G.W., Huang, X.P., Vardy, E., McCorvy, J.D.,
553 Jiang, Y., Chu, M., Siu, F.Y.*, et al.* (2013). Structural features for functional selectivity at
554 serotonin receptors. Science *340*, 615-619.

555 Wang, F., Beck-Garcia, K., Zorzin, C., Schamel, W.W., and Davis, M.M. (2016).
556 Inhibition of T cell receptor signaling by cholesterol sulfate, a naturally occurring
557 derivative of membrane cholesterol. Nat Immunol *17*, 844-850.

558 Wei, Q., Brzostek, J., Sankaran, S., Casas, J., Hew, L.S., Yap, J., Zhao, X., Wojciech,
559 L., and Gascoigne, N.R.J. (2020). Lck bound to coreceptor is less active than free Lck.
560 Proc Natl Acad Sci U S A *117*, 15809-15817.

561 Wu, L., Wei, Q., Brzostek, J., and Gascoigne, N.R.J. (2020). Signaling from T cell
562 receptors (TCRs) and chimeric antigen receptors (CARs) on T cells. Cell Mol Immunol
563 *17*, 600-612.

564 Xu, C., Gagnon, E., Call, M.E., Schnell, J.R., Schwieters, C.D., Carman, C.V., Chou,
565 J.J., and Wucherpfennig, K.W. (2008). Regulation of T cell receptor activation by
566 dynamic membrane binding of the CD3epsilon cytoplasmic tyrosine-based motif. Cell
567 *135*, 702-713.

568 Xu, H., and Littman, D.R. (1993). A kinase-independent function of Lck in potentiating
569 antigen-specific T cell activation. Cell *74*, 633-643.
570

571 **Figure Legends**
572
573 **Figure 1. Computational reconstruction of CD4 evolution.**
574 The maximum likelihood phylogenetic tree clusters mammalian CD4 sequences. The
575 tree highlights ancestral reconstructions of CD4 sequences from marsupials (kangaroo
576 silhouette), Atlantogenata (elephant), and Boreoeutheria (wildcat). The logoplot of
577 extant eutherian (Atlantogenata and Boreoeutheria) CD4 sequences show sequence
578 conservation over evolutionary time. In these plots, the height of symbols indicates the
579 relative frequency of each amino acid at that specific position. The mouse CD4
580 numbering (uniprot) is used as a reference, and residues are color-coded based on
581 sidechain polarity. Evolutionary insertion or deletion events are indicated by dashes (-).
582 Most recent common ancestor (MRCA) sequences are shown at each node in the tree
583 (Node 1-4). As in our previous study (Lee et al., 2022), the ratio of synonymous (dS)
584 and nonsynonymous (dN) substitution rates was calculated. Black dots indicate dN/dS
585 ratios that are significantly below 1 across the entire dataset. Red dots indicate residues
586 under purifying selection in the mammalian only dataset. Previously identified motifs are
587 indicated by boxes, while the intracellular domain helix is shaded gray. The arrow at
588 position 422 indicates where CD4 was truncated (CD4-T1), while TMD and T1-Palm
589 show the mutations studied in this study.
590
591 **Figure 2. Truncating CD4 does not reduce CD3ζ phosphorylation.**
592 (**A**) Representative IL-2 production is shown in response to a titration of MCC peptide
593 from one experiment (left). Experiments were performed in triplicate and each symbol
594 equals the mean +/- SEM at that peptide concentration. AUC analysis for the dose
595 response is shown as a measure of the response magnitude for the average of three
596 independent experiments performed with one independently generated set of cell lines
597 (center). The average response to a low dose (41nM) of peptide is shown as a measure
598 of sensitivity for three independent experiments performed with one independently
599 generated set of cell lines (right). The data are representative of those obtained with 4
600 (WT vs T1) or 2 (WT vs $T1^{\Delta bind}$) independently generated sets of cell lines.
601 (**B**) Phosphorylation intensity of CD3ζ (pCD3ζ) for WT and CD4-T1 (T1) (left),
602 normalized pCD3ζ intensity for WT and T1 (center), and normalized % responders of
603 pCD3ζ for WT and T1 (right). Five independently generated cell lines (biological
604 replicates) were tested for WT and T1. For phosphorylation intensity, each pair of lines
605 (connected symbols) was tested in three independent experiments. Data were analyzed
606 and collected as in Figure 2 – figure supplement 3. One-way ANOVA was performed
607 with a Dunnett's posttest using GraphPad Prism9. For normalized intensity and %
608 responders, all individual mutant cell line values were normalized to their paired control
609 values. Bars represent the mean +/- SEM. One-way ANOVA was performed with a
610 Sidak's posttest for specific comparisons of normalized values using GraphPad Prism9.
611 (**C**) Phosphorylation intensity of pCD3ζ for T1 and $T1^{\Delta bind}$ (left), normalized pCD3ζ
612 intensity for T1 and $T1^{\Delta bind}$ (center), and normalized % responders of pCD3ζ for T1 and
613 $T1^{\Delta bind}$ (right) were performed and analyzed as in B, with the exception that the open
614 symbols represent data from a single experiment whereas the closed symbols represent
615 aggregate data from three independent experiments. Two-tailed t tests were performed

616 to compare the single T1 vs T1$^{\Delta bind}$ samples as no other samples were collected in
617 parallel.
618
619 **Figure 2- figure supplement 1.**
620 Flow cytometry analysis of CD4 (left) and TCR (right) expression on 58$\alpha^-\beta^-$ hybridoma
621 cells. Parental 58$\alpha^-\beta^-$ hybridoma cells served as negative control for surface expression
622 (open black histogram trace).
623
624 **Figure 2- figure supplement 2.**
625 TCR (left) and CD4 (right) endocytosis after pMHCII engagement is shown for the
626 indicated cell lines after 16 hours coculture with APCs in the presence of 10μM MCC
627 peptide. The change in TCR and CD4 gMFI, as measured by flow cytometry, is shown
628 for each cell line relative to an equivalent sample cultured with APCs in the absence of
629 MCC peptide. Each data point represents the mean ± SEM for three independent
630 experiments. For endocytosis measurements were performed in triplicate for each
631 experiment. One-way ANOVA was performed with a Dunnett's posttest.
632
633 **Figure 2-figure supplement 3.**
634 Example of intracellular signaling analysis workflow.
635 (**A**) Flow cytometry analysis of WT 58$\alpha^-\beta^-$ hybridoma:M12 cell couples. Representative
636 dot plots are shown for TCRβ^{GFP+} CD4$^+$ 58$\alpha^-\beta^-$ hybridoma cells coupled to Tag-it Violet-
637 labeled M12s expressing the indicated tethered pMCHII Hb:I-E^k (left) and MCC:I-E^k
638 (center). Representative histograms of WT 58$\alpha^-\beta^-$ hybridoma cells coupled to M12 cells
639 transduced to express the indicated tethered pMHCII are shown for pCD3ζ intensity
640 (right). 10,000 coupled cells were collected per individual experiment.
641 (**B**) Flow cytometry analysis of T1 58$\alpha^-\beta^-$ hybridoma-M12 cell couples. Representative
642 dot plots are shown for TCRβ^{GFP+} CD4$^+$ 58$\alpha^-\beta^-$ hybridoma cells coupled to Tag-it Violet-
643 labeled Hb:I-E^{k+} (left) and MCC:I-E^{k+} (center) M12 cells. Representative histograms of
644 T1 58$\alpha^-\beta^-$ hybridoma cells coupled to M12 cells expressing the indicated tethered
645 pMHCII are shown for pCD3ζ intensity (right). 10,000 coupled cells were collected per
646 individual experiment.
647 (**C**) A representative smoothed overlapping histogram of pCD3ζ intensity is shown for
648 58$\alpha^-\beta^-$ cells coupled to Hb:I-E^{k+} (cyan) or MCC:I-E^{k+} (black) M12 cells. Histogram of
649 pCD3ζ intensity for 58$\alpha^-\beta^-$ cells coupled to MCC:I-E^{k+} M12 cells subtracted from Hb:I-
650 E^{k+} M12 cell couples show the difference in pCD3ζ intensity on a bin-by-bin basis after
651 stimulation with agonist MCC:I-E^k compared with null Hb:I-E^k for WT (left) and T1
652 (center) cells. Overlapping pCD3ζ histogram (right) of cells responding to MCC:I-E^k
653 after Hb:I-E^k subtraction shows the responding populations for the WT and T1 cell lines.
654 Data represent the aggregate from three individual experiments (30,000 couples
655 analyzed). One-way ANOVA was performed with a Dunnett's posttest for comparison
656 with the WT sample because other mutants were simultaneously analyzed in this
657 experiment (not shown).
658 (**D**) Concatenated pCD3ζ average intensity ± SEM of WT and T1 cells (left) and the
659 percent of responding WT and T1 cells (right).
660

Figure 2-figure supplement 4.
(**A**) Zap70 (left), and Plcγ1 (right) phosphorylation intensity for WT and T1 are shown for paired (connecting line) WT and T1 cell lines. Five independently generated cell lines were tested (biological replicates). For phosphorylation intensity, each pair of lines (connected symbols) was tested in three independent experiments (technical replicates). The data from those experiments was aggregated, and the symbols represent the mean intensity of the aggregated pCD3ζ intensity values. One-way ANOVA was performed with a Dunnett's posttest.
(**B**) Average T1 phosphorylation for Zap70 (left) and Plcγ1 (right) from A are shown normalized to the paired WT controls. Bars represent the mean +/- SEM. One-way ANOVA was performed with a Sidak's posttest for specific comparisons.
(**C**) Average T1 % responders for pZap70 (left), and pPlcγ1 (right) are shown normalized to the paired WT controls for the cell lines shown in A. Bars represent the mean +/- SEM. One-way ANOVA was performed with a Sidak's posttest for specific comparisons.

Figure 2-figure supplement 5.
(**A**) Phosphorylation intensity for T1 and $T1^{\Delta bind}$ Zap70 (left), and Plcγ1 (right) are shown for paired (connecting line) T1 and $T1^{\Delta bind}$ cell lines. Three independently generated cell lines were tested (biological replicates). Analysis was performed as in Figure 2— figure supplement 4 with the exception that the open symbol represent data from a single experiment whereas the closed symbols represent the average of aggregated data from three independent experiments. For the open symbol comparisons we performed a two-tailed t test as no other samples were collected in parallel.
(**B**) Average $T1^{\Delta bind}$ cell line phosphorylation intensity for Zap70 (left), and Plcγ1 (right) are shown normalized to the average intensity of the paired T1 control cells shown in A. Analysis was performed as in Figure 2— figure supplement 4.
(**C**) Average $T1^{\Delta bind}$ cell line % responders for pZap70 (left) and pPlcγ1 (right) are shown normalized to their paired T1 control. Analysis was performed as in Figure 2— figure supplement 4.

Figure 3. The GGXXG and CV+C motifs are key determinants of CD4 function.
(**A, B**) Representative IL-2 production is shown in response to a titration of MCC peptide from one experiment (left). Experiments were performed in triplicate and each symbol equals the mean +/- SEM at that peptide concentration. AUC analysis for the dose response is shown as a measure of the response magnitude for the average of three independent experiments performed with one independently generated set of cell lines (center). The average response to a low dose (41nM) of peptide is shown as a measure of sensitivity for three independent experiments performed with one independently generated set of cell lines (right). Results are representative of those obtained with at least three independently generated sets of cell lines. One-way ANOVA was performed with a Dunnett's posttest for comparisons with WT and T1 samples, and a Sidak's posttest for comparisons between selected samples.

Figure 3- figure supplement 1.

706 (**A, B**) Flow cytometry analysis of CD4 (left) and TCR (right) expression on $58\alpha^-\beta^-$
707 hybridoma cells. Parental $58\alpha^-\beta^-$ hybridoma cells served as negative control for surface
708 expression (open black histogram trace).
709
710 **Figure 3- figure supplement 2.**
711 (**A, B**) Lck signal is shown for each sucrose fraction normalized to the CD4 signal
712 detected in the corresponding fraction (left). The AUC is shown for the normalized Lck
713 signal in the DRM (center) and DSM (right) fractions. Each data point represents the
714 mean +/- SEM for three independent experiments with the same cell line. Data are
715 representative of experiments performed with three independently generated sets of
716 lines for TMD, Palm(3C), and TP(3C) mutants. Analysis was performed with two set of
717 lines for the Palm(2C) and TP(2C) mutants. One-way ANOVA was performed with a
718 Dunnett's posttest for comparisons with WT and T1 samples, and a Sidak's posttest for
719 comparisons between selected samples.
720
721 **Figure 3- figure supplement 3.**
722 (**A, B**) Total Lck signal (total AUC for sucrose gradient) normalized to CD4 signal is
723 shown for the indicated cell lines. Each data point represents the mean +/- SEM for
724 three independent experiments with the same cell line (experimental replicates). Data
725 are representative of experiments performed with three independently generated sets of
726 lines for TMD, Palm(3C), and TP(3C) mutants (biological replicates). Analysis was
727 performed with two set of lines for the Palm(2C) and TP(2C) mutants. One-way ANOVA
728 was performed with a Dunnett's posttest for comparisons with WT and T1 samples, and
729 a Sidak's posttest for comparisons between selected samples.
730
731 **Figure 3- figure supplement 4.**
732 (**A, B**) TCR (left) and CD4 (right) endocytosis after pMHCII engagement is shown for
733 the indicated cell lines after 16 hours coculture with APCs in the presence of 10μM
734 MCC peptide. The change in TCR and CD4 gMFI, as measured by flow cytometry, is
735 shown for each cell line relative to an equivalent sample cultured with APCs in the
736 absence of MCC peptide. Each data point represents the mean ± SEM for three
737 independent experiments (experimental replicates). Data are representative of those
738 acquired with at least two independently generated sets of cell lines (biological
739 replicates). Endocytosis measurements were performed in triplicate (technical
740 replicates) for each experiment. One-way ANOVA was performed with a Dunnett's
741 posttest for comparisons with WT and T1 samples.
742
743 **Figure 4. The GGXXG and CV+C motifs reduce pCD3ζ levels.**
744 (**A**) Phosphorylation intensity of CD3ζ for T1 and T1-TMD (left), T1 and T1-Palm (2C)
745 (center), and T1 and T1-TP (2C) (right) are shown for independently generated pairs of
746 (connecting line) T1 and T1-TMD (left), T1 and T1-Palm (2C) (center), and T1 and T1-
747 TP (2C) (right) cell lines. Each pair of lines (connected closed symbols) was tested in
748 three independent experiments (technical replicates). The data from those experiments
749 was aggregated, and the symbols represent the mean intensity of the aggregated
750 pCD3ζ intensity values. One-way ANOVA was performed with a Dunnett's posttest
751 using GraphPad Prims 9.

752 (**B**) Data for each cell line in **A** are shown as the average pCD3ζ intensity for all T1-
753 TMD (left), T1-Palm (2C) (center), and T1-TP (2C) (right) cell lines normalized to their
754 paired T1 control. Dotted line is the normalized pCD3ζ intensity for $T1^{\Delta bind}$ as a visual
755 reference point for the contributions of CD4-pMHCII interactions. Bars represent the
756 mean +/- SEM. One-way ANOVA was performed with a Sidak's posttest for specific
757 comparisons using GraphPad Prims 9.
758 (**C**) The average % responders for phosphorylation of CD3ζ is shown for T1-TMD (left),
759 T1-Palm (2C) (center), and T1-TP (2C) (right) normalized to their paired T1 control line.
760 Bars represent the mean +/- SEM. One-way ANOVA was performed with a Sidak's
761 posttest for specific comparisons using GraphPad Prims 9.
762
763 **Figure 4- figure supplement 1.**
764 (**A**) Phosphorylation intensity of Zap70 for T1 and T1-TMD (left), T1 and T1-Palm (2C)
765 (center), and T1 and T1-TP (2C) (right) are shown for paired (connecting line) cell lines.
766 Analysis was performed as in Figure 4A.
767 (**B**) Normalized phosphorylation intensity of Zap70 for T1-TMD (left), T1-Palm (2C)
768 (center), and T1-TP (2C) (right) are shown as bars. Analysis was performed as in Figure
769 4B.
770 (**C**) Normalized % responders of the phosphorylation Zap70 for T1-TMD (left), T1-Palm
771 (2C) (center), and T1-TP (2C) (right) are shown as bars for T1 and $T1^{\Delta bind}$ cell lines.
772 Analysis was performed as in Figure 4C.
773
774 **Figure 4- figure supplement 2.**
775 (**A**) Phosphorylation intensity of Plcγ1 for T1 and T1-TMD (left), T1 and T1-Palm (2C)
776 (center), and T1 and T1-TP (2C) (right) are shown for paired (connecting line) cell lines.
777 Analysis was performed as in Figure 4A.
778 (**B**) Normalized phosphorylation intensity of Plcγ1 for T1-TMD (left), T1-Palm (2C)
779 (center), and T1-TP (2C) (right) are shown as bars. Analysis was performed as in Figure
780 4B.
781 (**C**) Normalized % responders of phosphorylated pPlcγ1 for T1-TMD (left), T1-Palm (2C)
782 (center), and T1-TP (2C) (right) are shown as bars for T1 and $T1^{\Delta bind}$ cell lines. Analysis
783 was performed as in Figure 4C.
784
785 **Figure 4- figure supplement 3.** Representative IL-2 production is shown in response to
786 M12 cells transduced to express tethered MCC:I-E^k constructs as used in
787 phosphorylation analysis. Experiments were performed in triplicate and each bar equals
788 the mean +/- SEM at that peptide concentration. Results are representative of those
789 obtained with two independently generated matched sets of cell lines. One-way ANOVA
790 was performed with a Dunnett's posttest for comparisons with WT and T1 samples, and
791 a Sidak's posttest for comparisons between selected samples.
792
793 **Figure 5. The (C/F)CVRC motifs reduces proximal TCR-CD3 signaling.**
794 (**A**) Phosphorylation intensity of CD3ζ for T1 and T1-Palm (3C) (left) and T1 and T1-TP
795 (3C) (right) are shown for independently generated pairs of (connecting lines) T1 and
796 T1-Palm (3C) (left) and T1 and T1-TP (3C) (right) cell lines. Analysis was performed as
797 in Figure 4A.

(**B**) Data for each mutant cell line in **A** are shown as the average pCD3ζ intensity values for T1-Palm (3C) (left) and T1-TP (3C) (right) normalized to their paired T1 controls. The dotted line represents the normalized phosphorylation CD3ζ intensity for $T1^{\Delta bind}$ as a visual reference for the contributions of CD4-pMHCII interactions. Analysis was performed as in Figure 4C.
(**C**) Average % responders for phosphorylation of CD3ζ is shown for T1-Palm (3C) (left) and T1-TP (3C) (right) normalized to their paired T1 control. Analysis was performed as in Figure 4C.

Figure 5- figure supplement 1.
(**A**) Phosphorylation intensity of Zap70 for T1 and T1-Palm (3C) (left) and T1 and T1-TP (3C) (right) are shown for paired (connecting line) cell lines. Analysis was performed as in Figure 5A.
(**B**) Normalized phosphorylation intensity of Zap70 for T1-Palm (3C) (left) and T1-TP (3C) (right) are shown as bars. Analysis was performed as in Figure 5B.
(**C**) Normalized % responders of phosphorylated Zap70 for T1-Palm (3C) (left) and T1-TP (3C) (right) are shown as bars. Analysis was performed as in Figure 5C.

Figure 5- figure supplement 2.
(**A**) Phosphorylation intensity of Plcγ1 for T1 and T1-Palm (3C) (left) and T1 and T1-TP (3C) (right) are shown for paired (connecting line) cell lines. Analysis was performed as in Figure 5A.
(**B**) Normalized phosphorylation intensity of Plcγ1 for T1-Palm (3C) (left) and T1-TP (3C) (right) are shown as bars. Analysis was performed as in Figure 5B.
(**C**) Normalized % responders of phosphorylated Plcγ1 for T1-Palm (3C) (left) and T1-TP (3C) (right) are shown as bars. Analysis was performed as in Figure 5C.

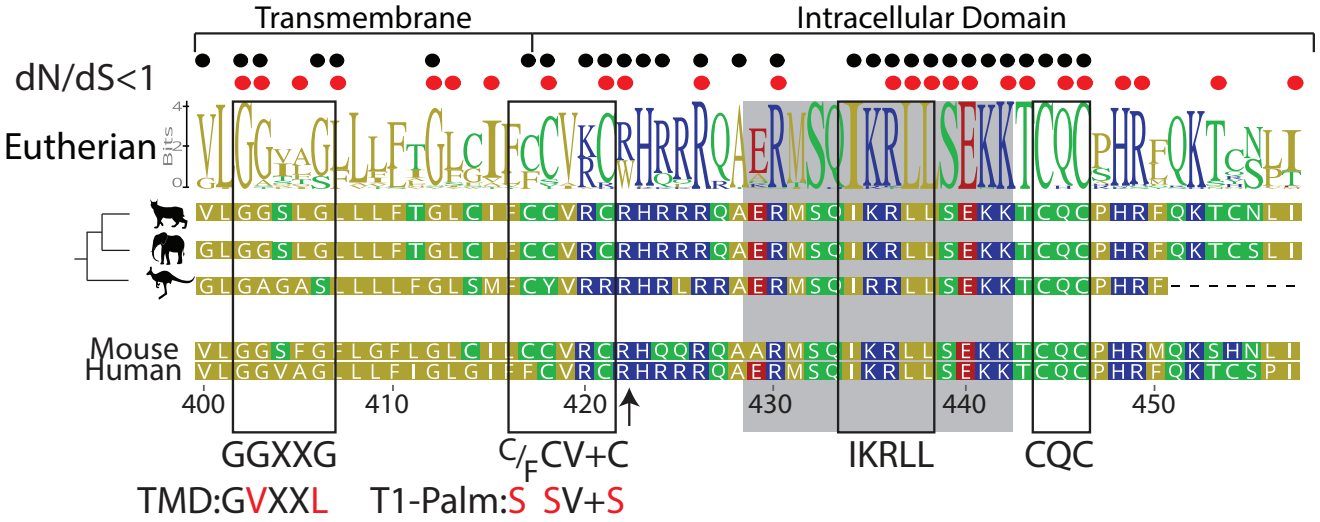
Transmembrane
Intracellular Domain
dN/dS<1
Eutherian
Bits
Mouse
Human
400
410
420
430
440
450
GGXXG
C/F CV+C
IKRLL
CQC
TMD:GVXXL
T1-Palm:S SV+S

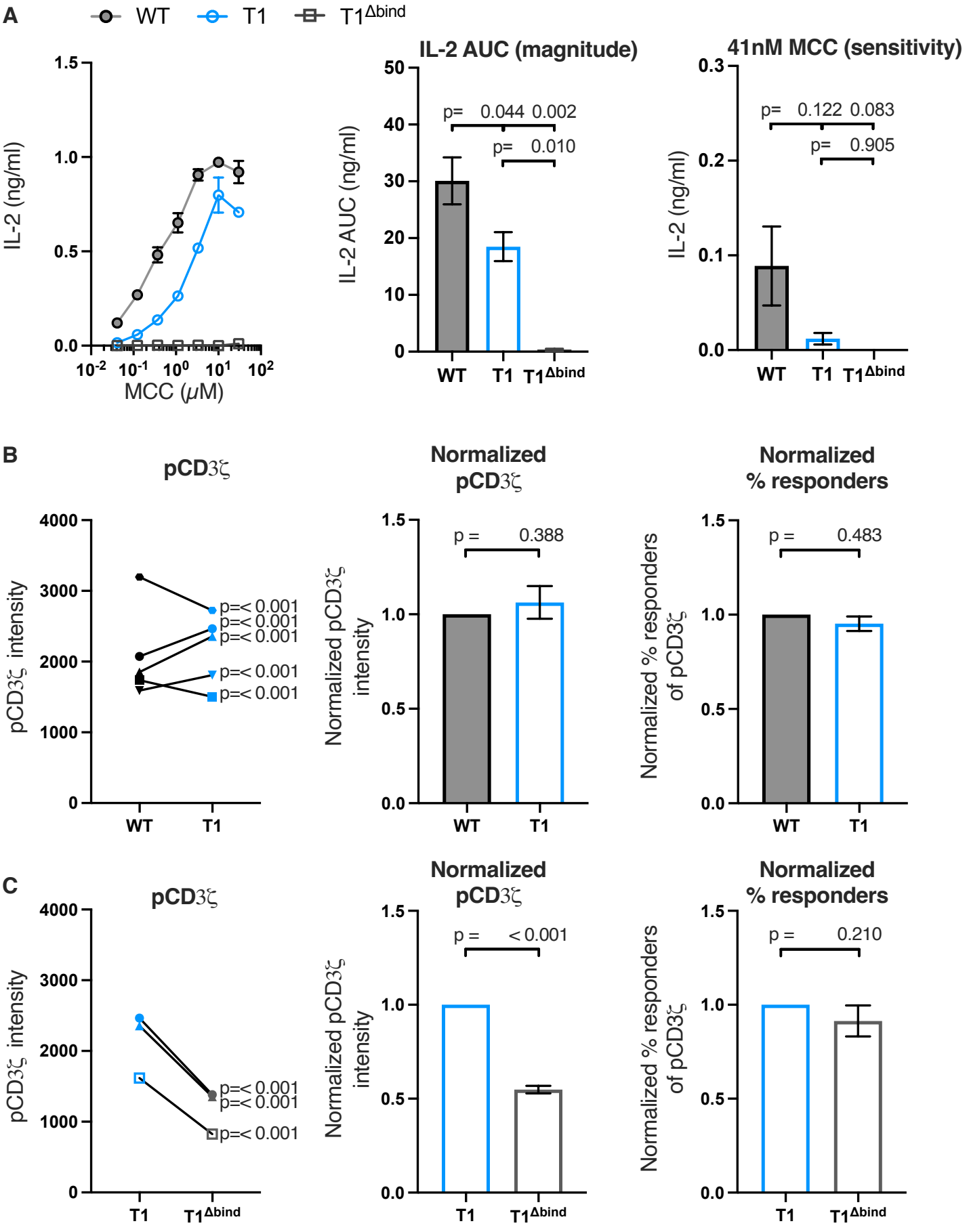
A
WT
T1
T1Δbind
IL-2 (ng/ml)
MCC (μM)
IL-2 AUC (magnitude)
IL-2 AUC (ng/ml)
p= 0.044 0.002
p= 0.010
41nM MCC (sensitivity)
p= 0.122 0.083
p= 0.905
B
pCD3ζ
pCD3ζ intensity
p=< 0.001
Normalized pCD3ζ
Normalized pCD3ζ intensity
p = 0.388
Normalized % responders
Normalized % responders of pCD3ζ
p = 0.483
C
p = < 0.001
p = 0.210

Figure 2

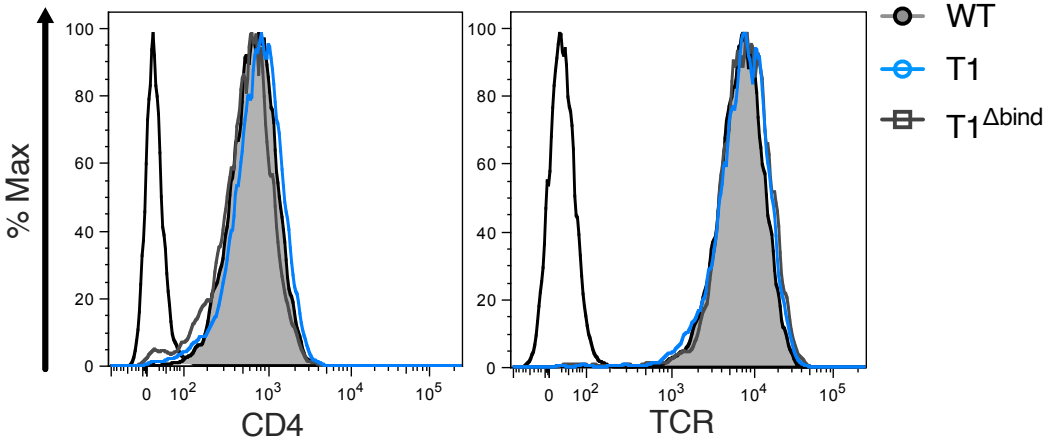

Figure 2 — figure supplement 1

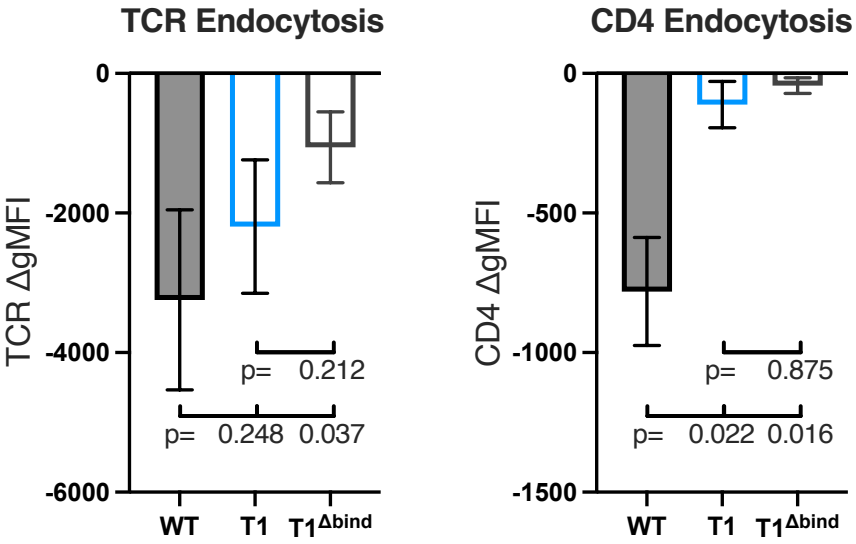

Figure 2 — figure supplement 2

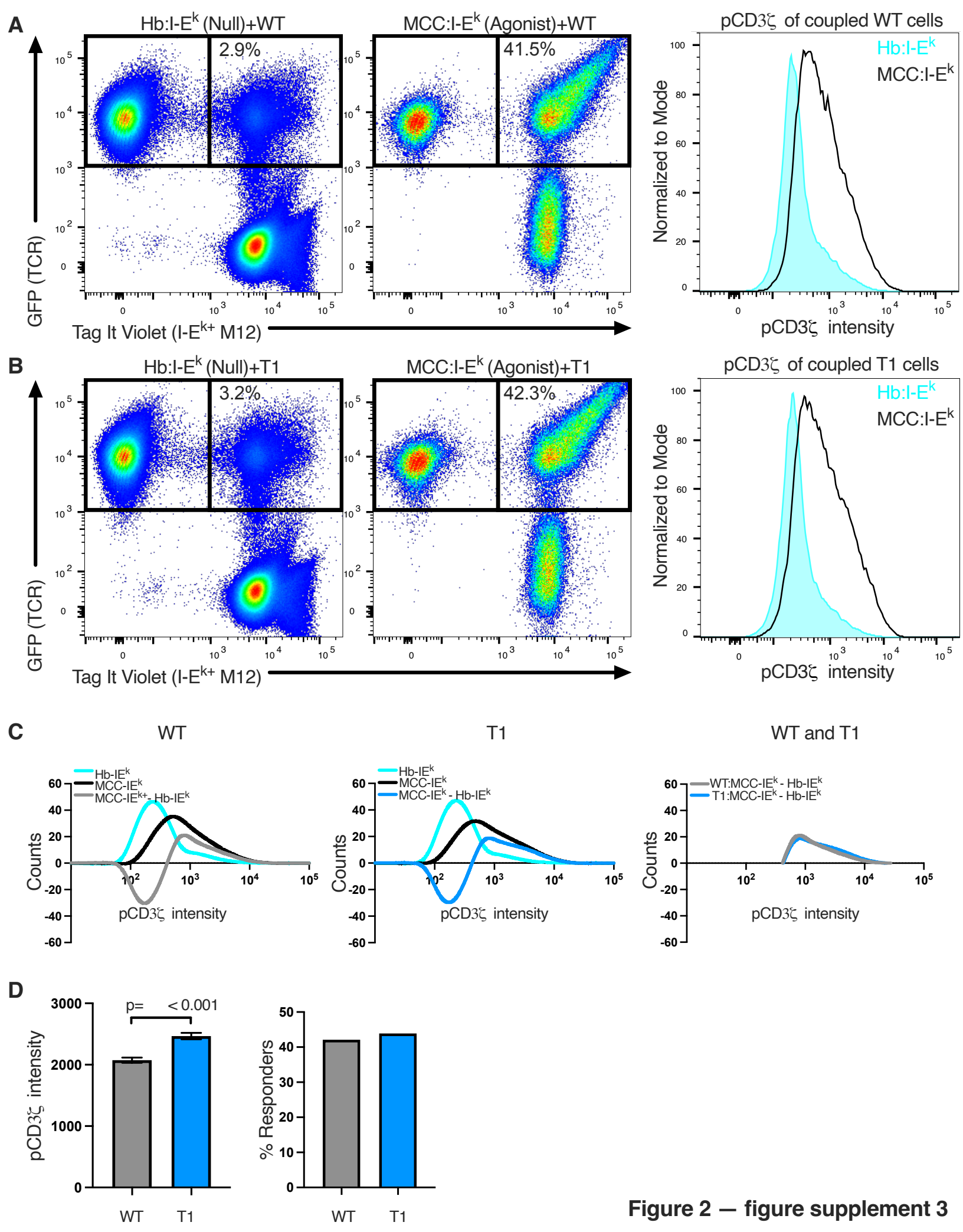

Figure 2 — figure supplement 3

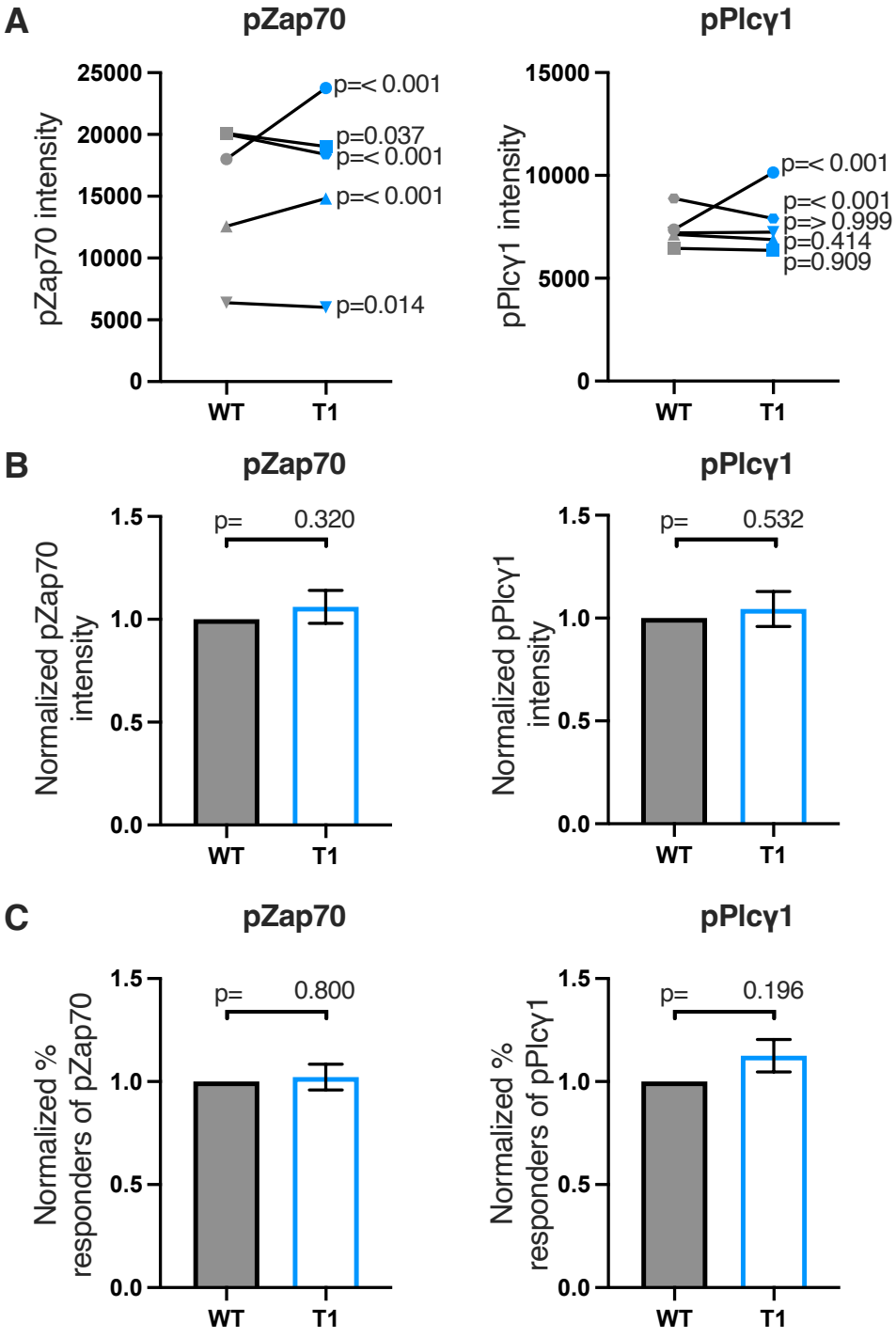

Figure 2 — figure supplement 4

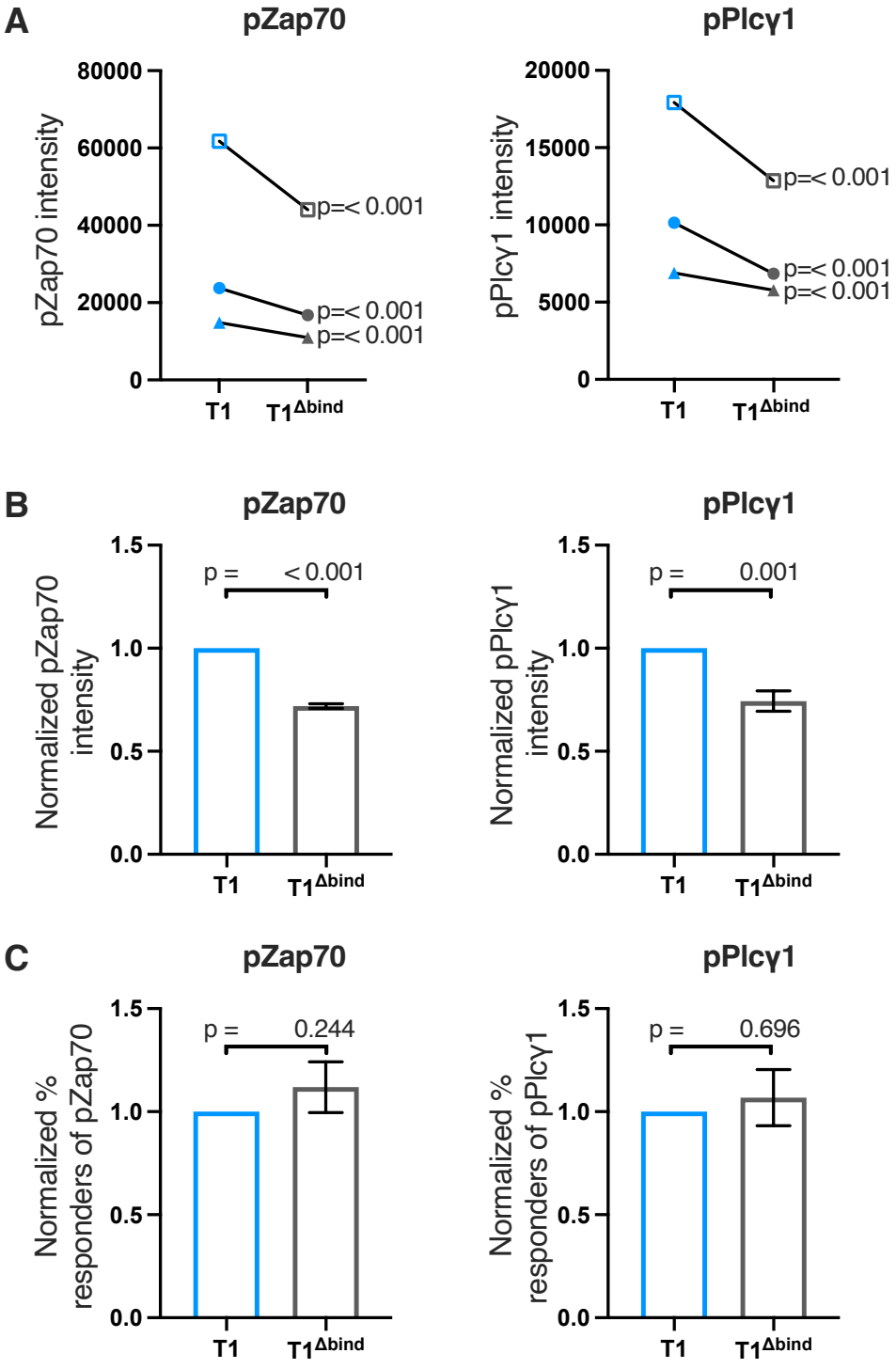

Figure 2 — figure supplement 5

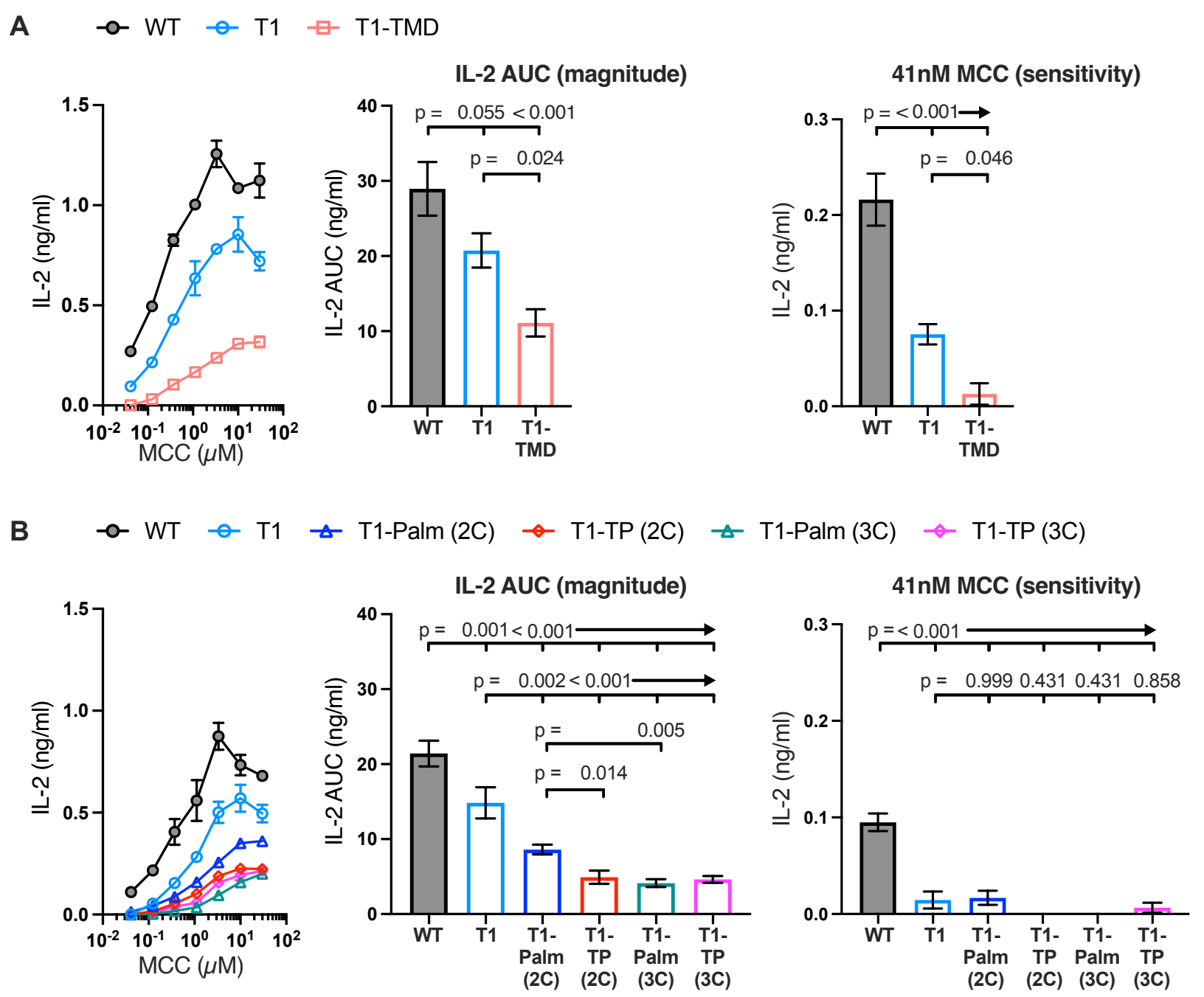
A
WT
T1
T1-TMD
IL-2 (ng/ml)
MCC (μM)
IL-2 AUC (magnitude)
IL-2 AUC (ng/ml)
p = 0.055
< 0.001
p = 0.024
WT
T1
T1-TMD
41nM MCC (sensitivity)
p = < 0.001
p = 0.046
B
WT
T1
T1-Palm (2C)
T1-TP (2C)
T1-Palm (3C)
T1-TP (3C)
p = 0.001
< 0.001
p = 0.002
< 0.001
p = 0.005
p = 0.014
p = < 0.001
p = 0.999 0.431 0.431 0.858

Figure 3

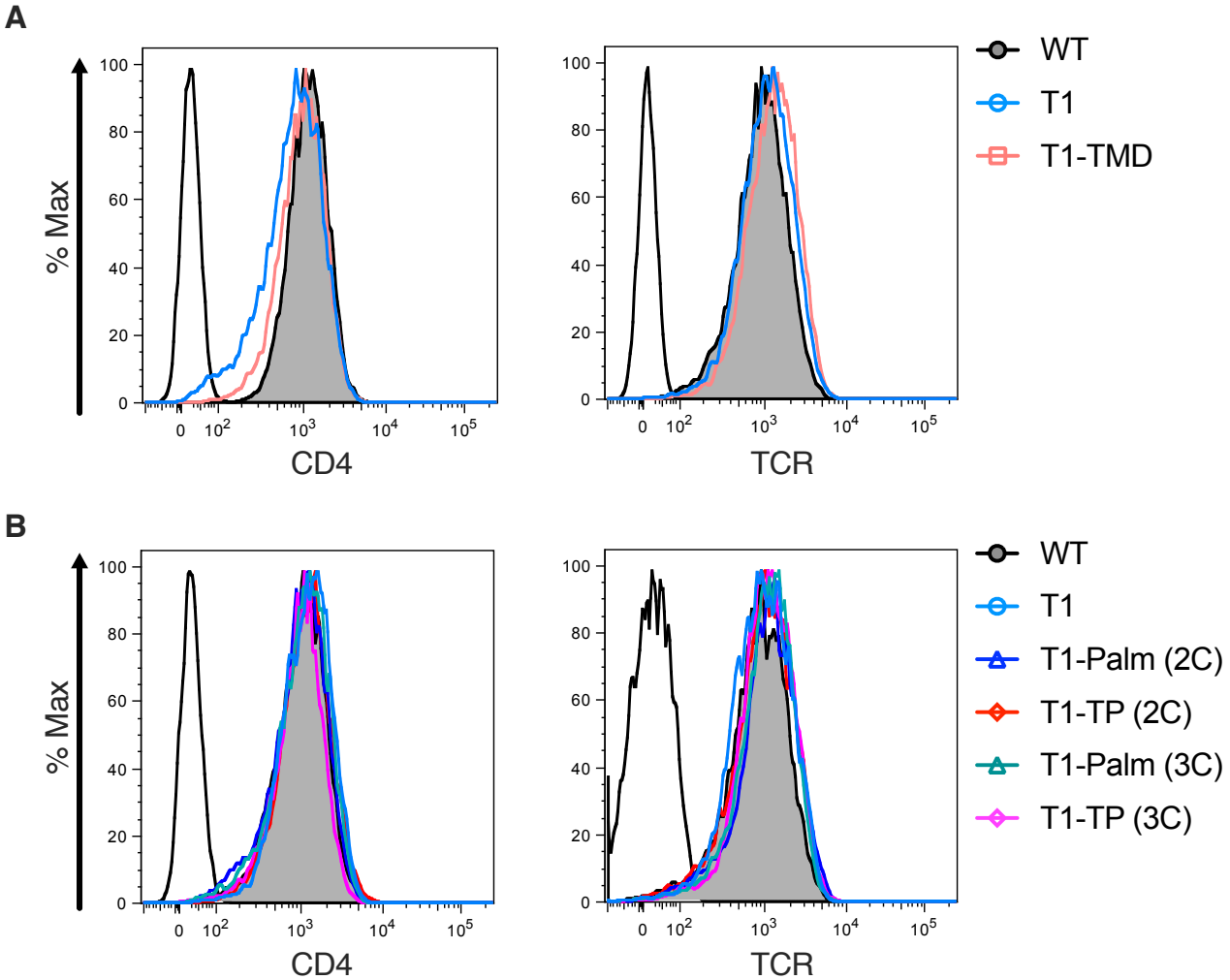

Figure 3 — figure supplement 1

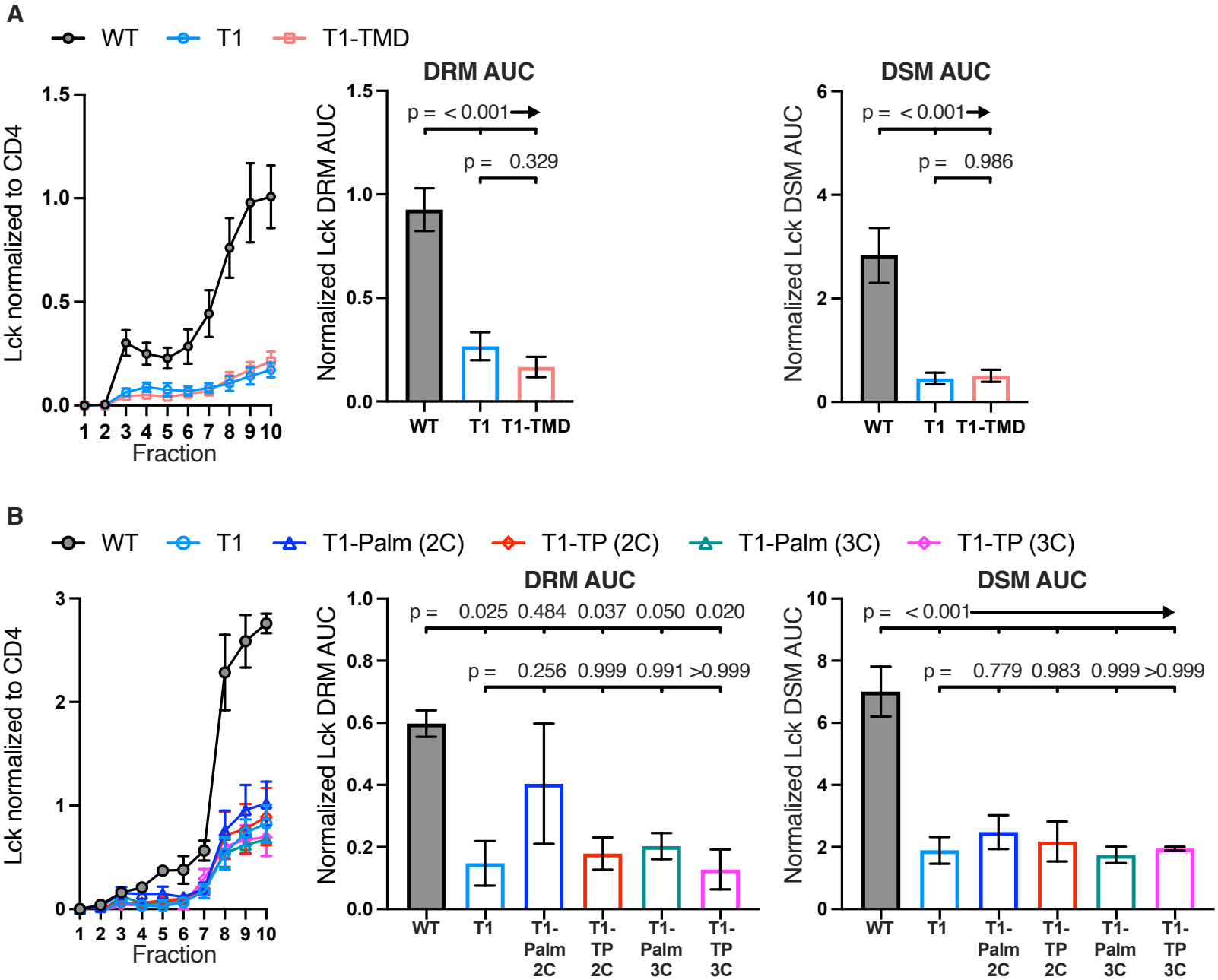

Figure 3 — figure supplement 2

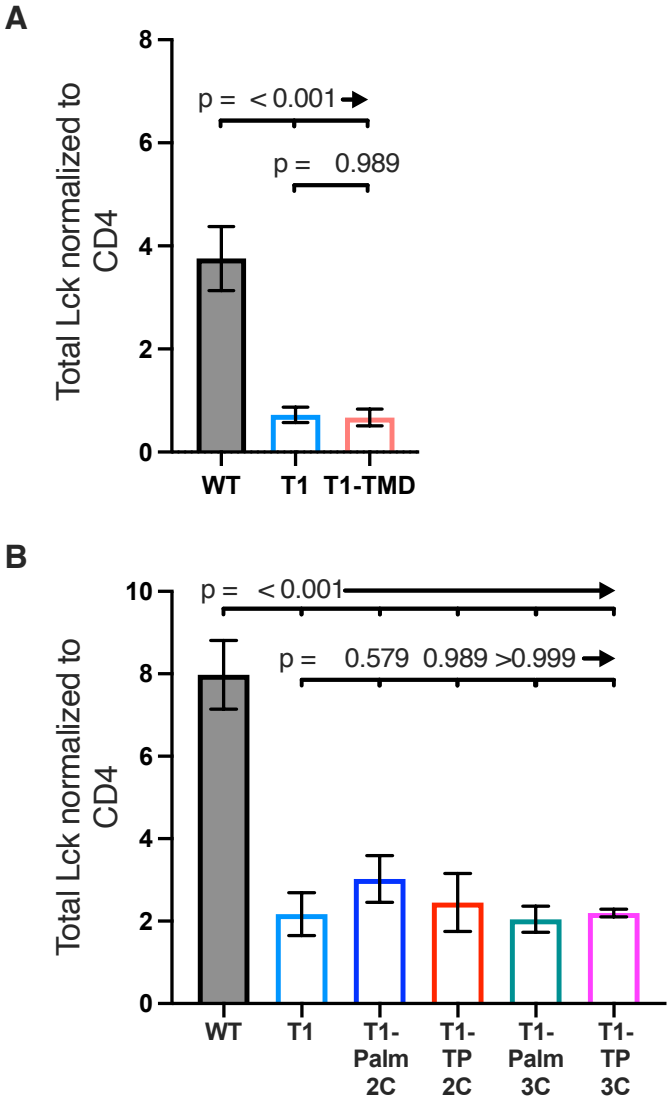

Figure 3 — figure supplement 3

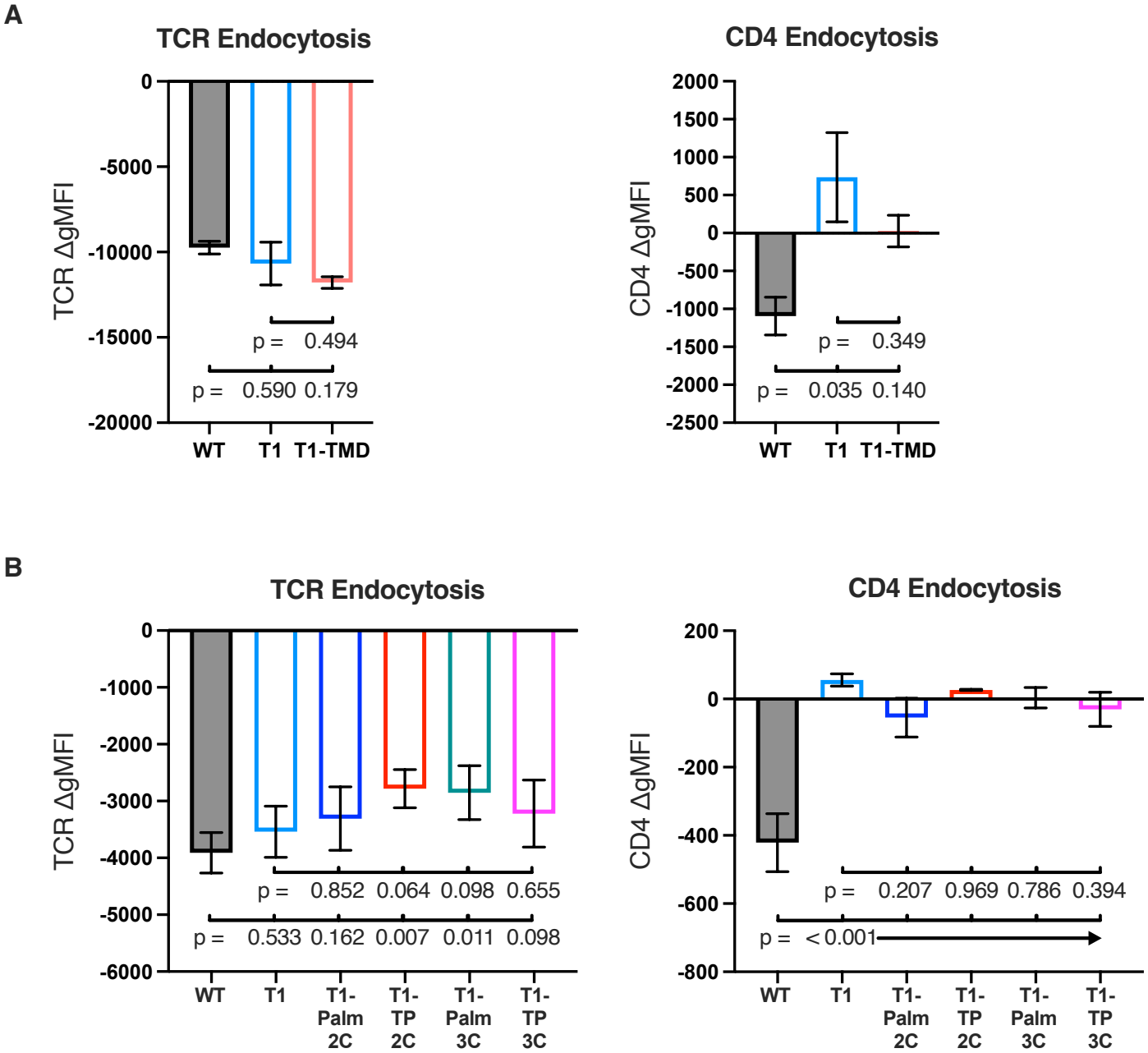

Figure 3 — figure supplement 4

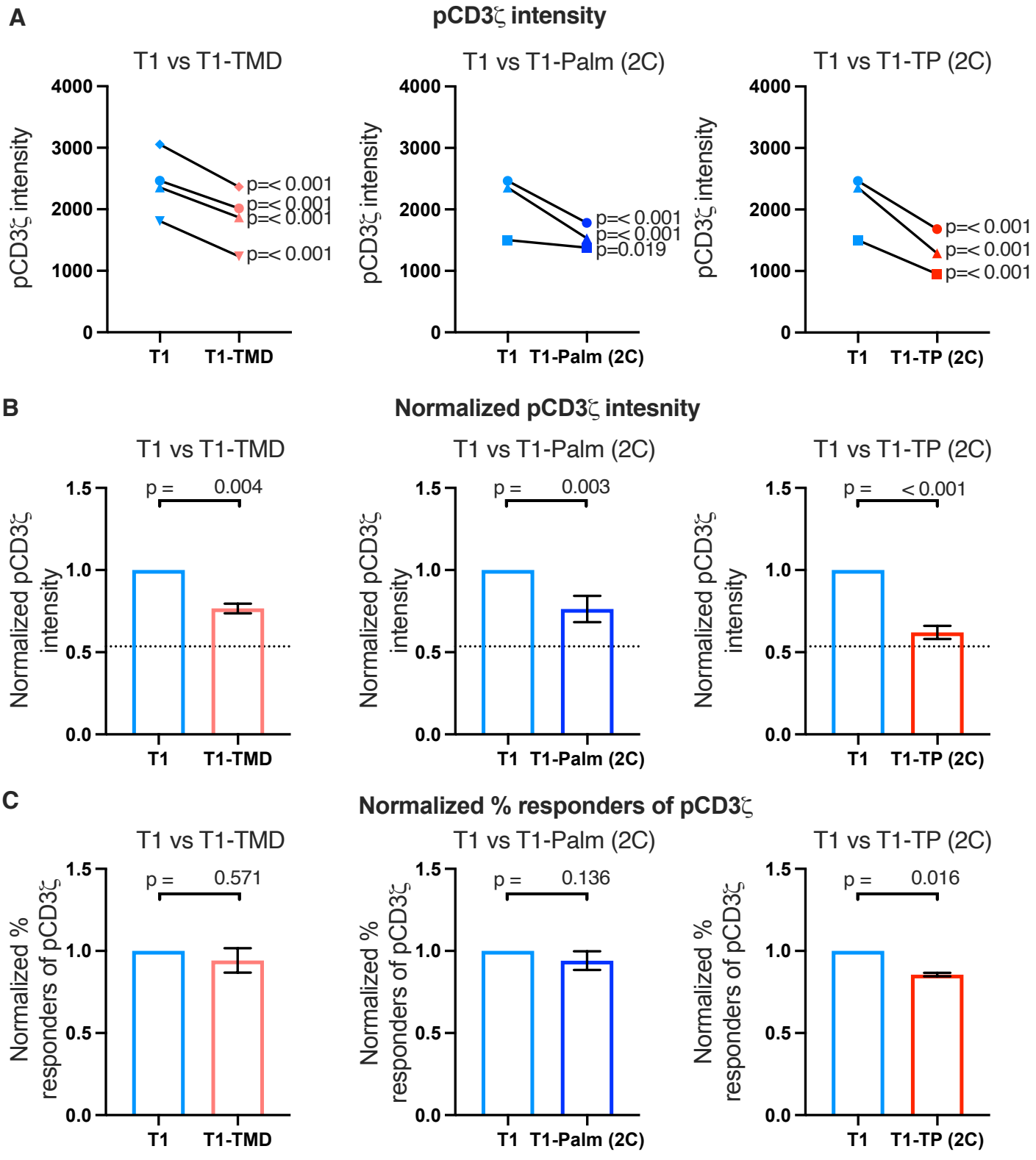
A
pCD3ζ intensity
T1 vs T1-TMD
T1 vs T1-Palm (2C)
T1 vs T1-TP (2C)
pCD3ζ intensity
4000
3000
2000
1000
0
p=< 0.001
p=< 0.001
p=< 0.001
p=< 0.001
p=< 0.001
p=< 0.001
p=0.019
p=< 0.001
p=< 0.001
p=< 0.001
T1
T1-TMD
T1-Palm (2C)
T1-TP (2C)
B
Normalized pCD3ζ intesnity
T1 vs T1-TMD
T1 vs T1-Palm (2C)
T1 vs T1-TP (2C)
Normalized pCD3ζ intensity
1.5
1.0
0.5
0.0
p = 0.004
p = 0.003
p = < 0.001
T1
T1-TMD
T1-Palm (2C)
T1-TP (2C)
C
Normalized % responders of pCD3ζ
T1 vs T1-TMD
T1 vs T1-Palm (2C)
T1 vs T1-TP (2C)
Normalized % responders of pCD3ζ
1.5
1.0
0.5
0.0
p = 0.571
p = 0.136
p = 0.016
T1
T1-TMD
T1-Palm (2C)
T1-TP (2C)

Figure 4

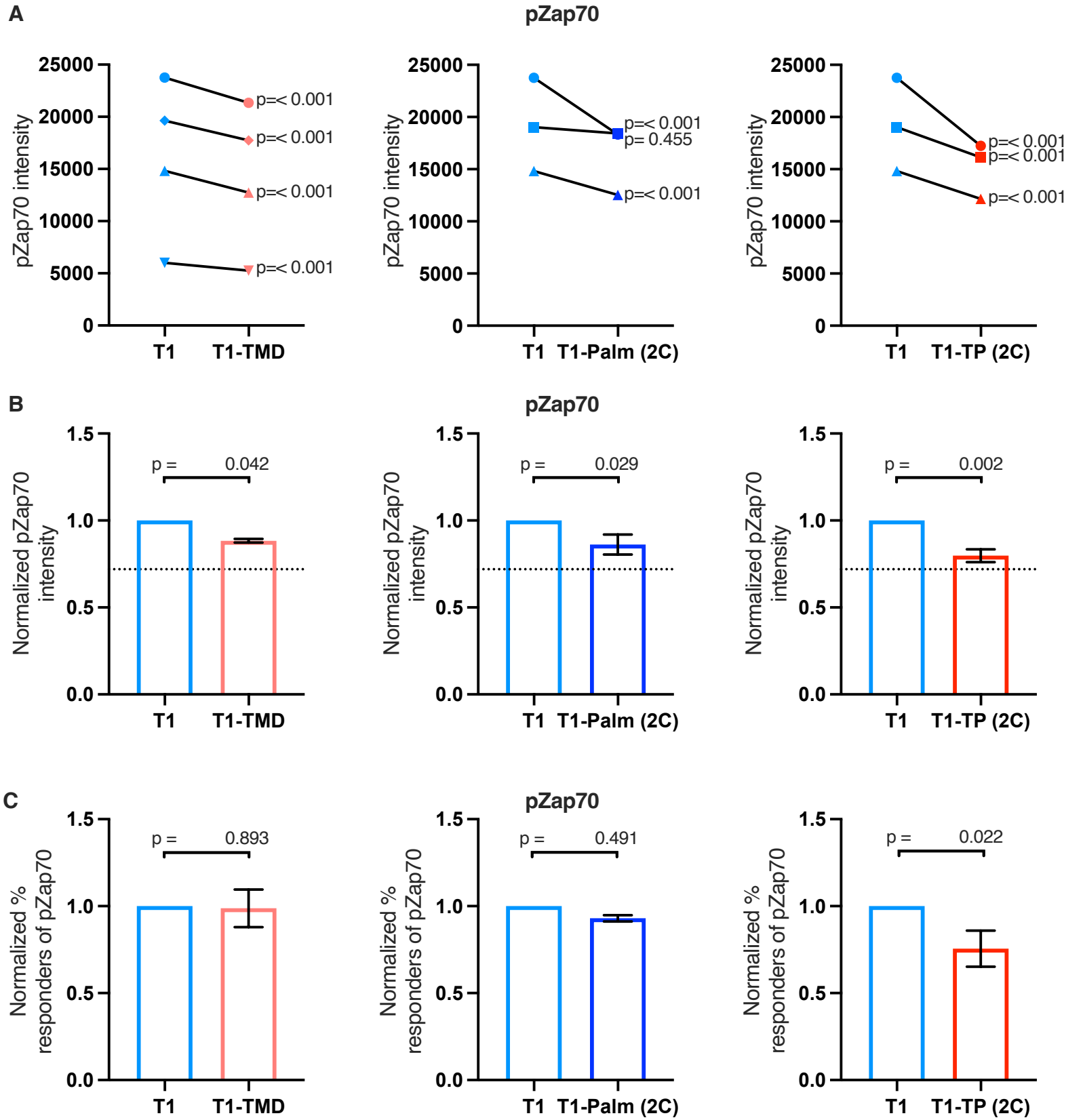

Figure 4 — figure supplement 1

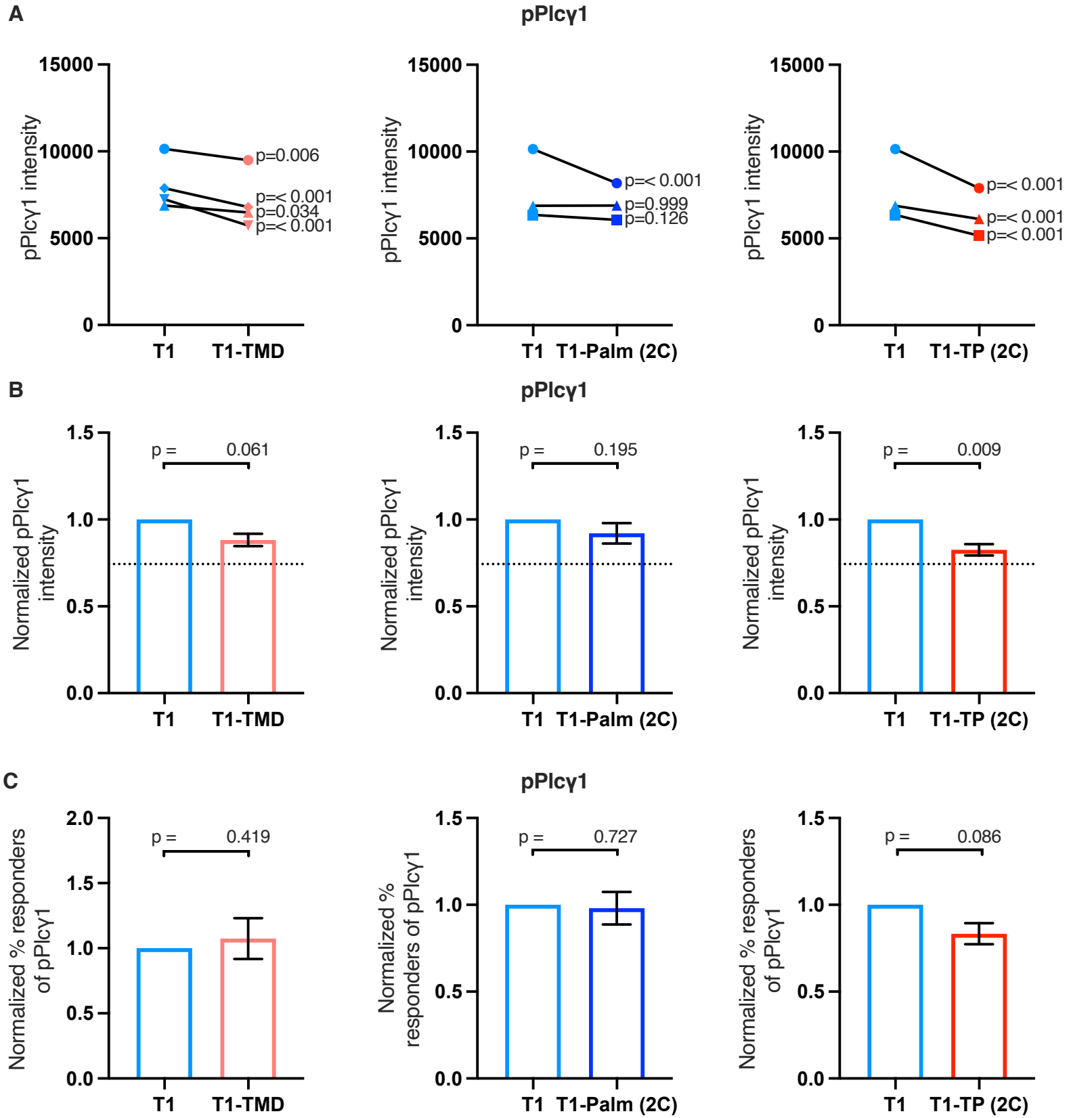

Figure 4 — figure supplement 2

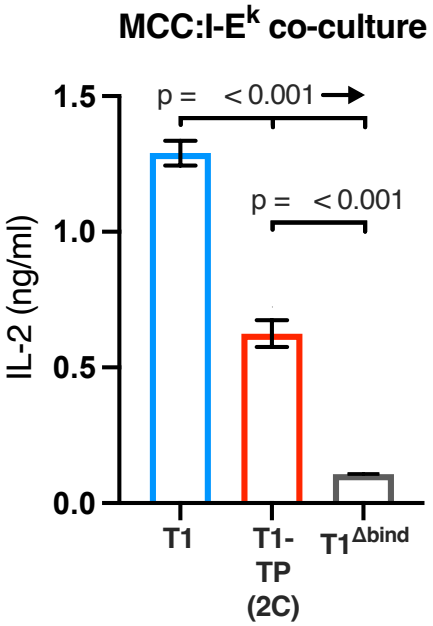

Figure 4 — figure supplement 3

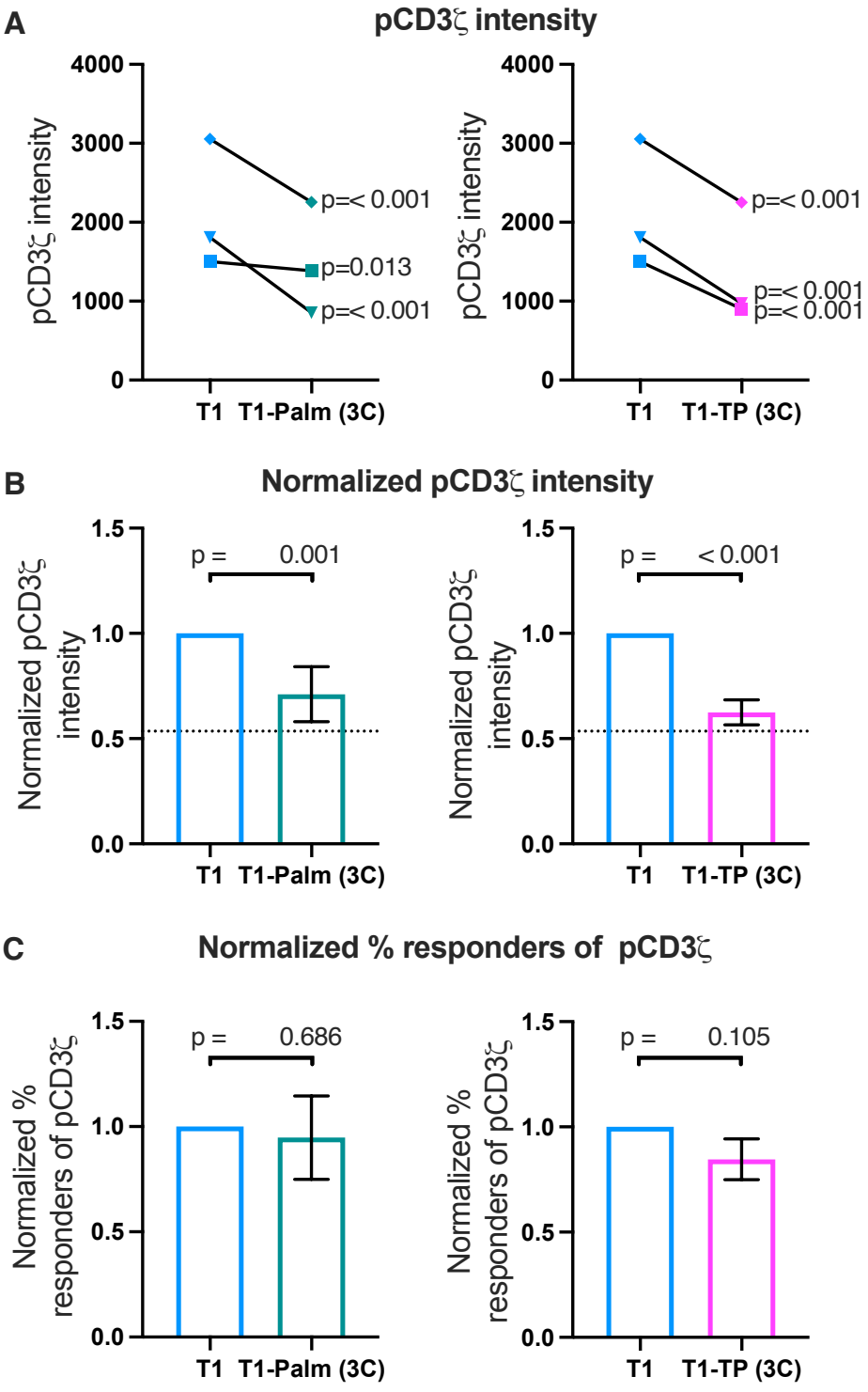
A
pCD3ζ intensity
pCD3ζ intensity
4000
3000
2000
1000
0
p=< 0.001
p=0.013
p=< 0.001
T1
T1-Palm (3C)
p=< 0.001
p=< 0.001
p=< 0.001
T1
T1-TP (3C)
B
Normalized pCD3ζ intensity
Normalized pCD3ζ intensity
1.5
1.0
0.5
0.0
p = 0.001
T1
T1-Palm (3C)
p = < 0.001
T1
T1-TP (3C)
C
Normalized % responders of pCD3ζ
Normalized % responders of pCD3ζ
p = 0.686
T1
T1-Palm (3C)
p = 0.105
T1
T1-TP (3C)

Figure 5

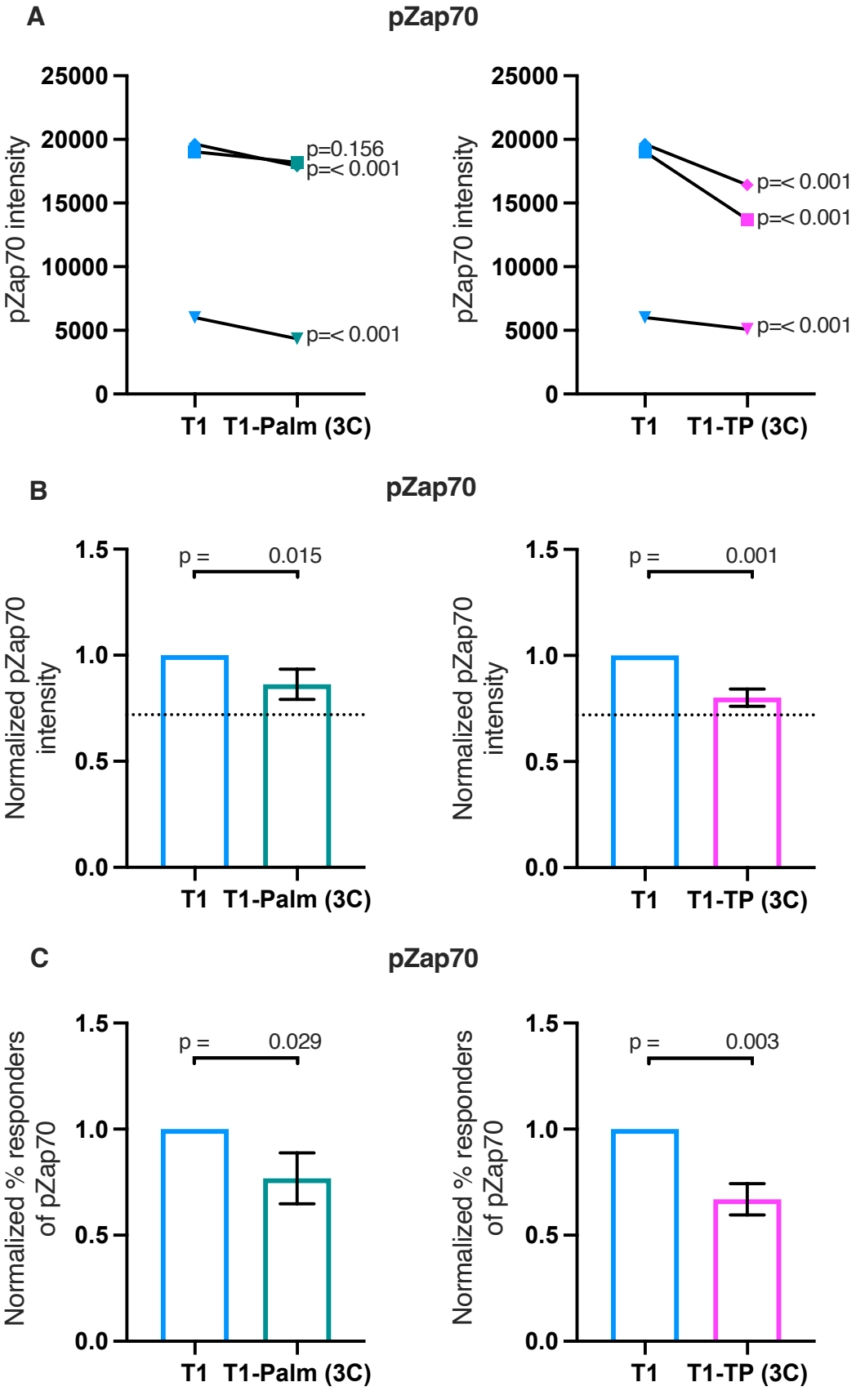

Figure 5 — figure supplement 1

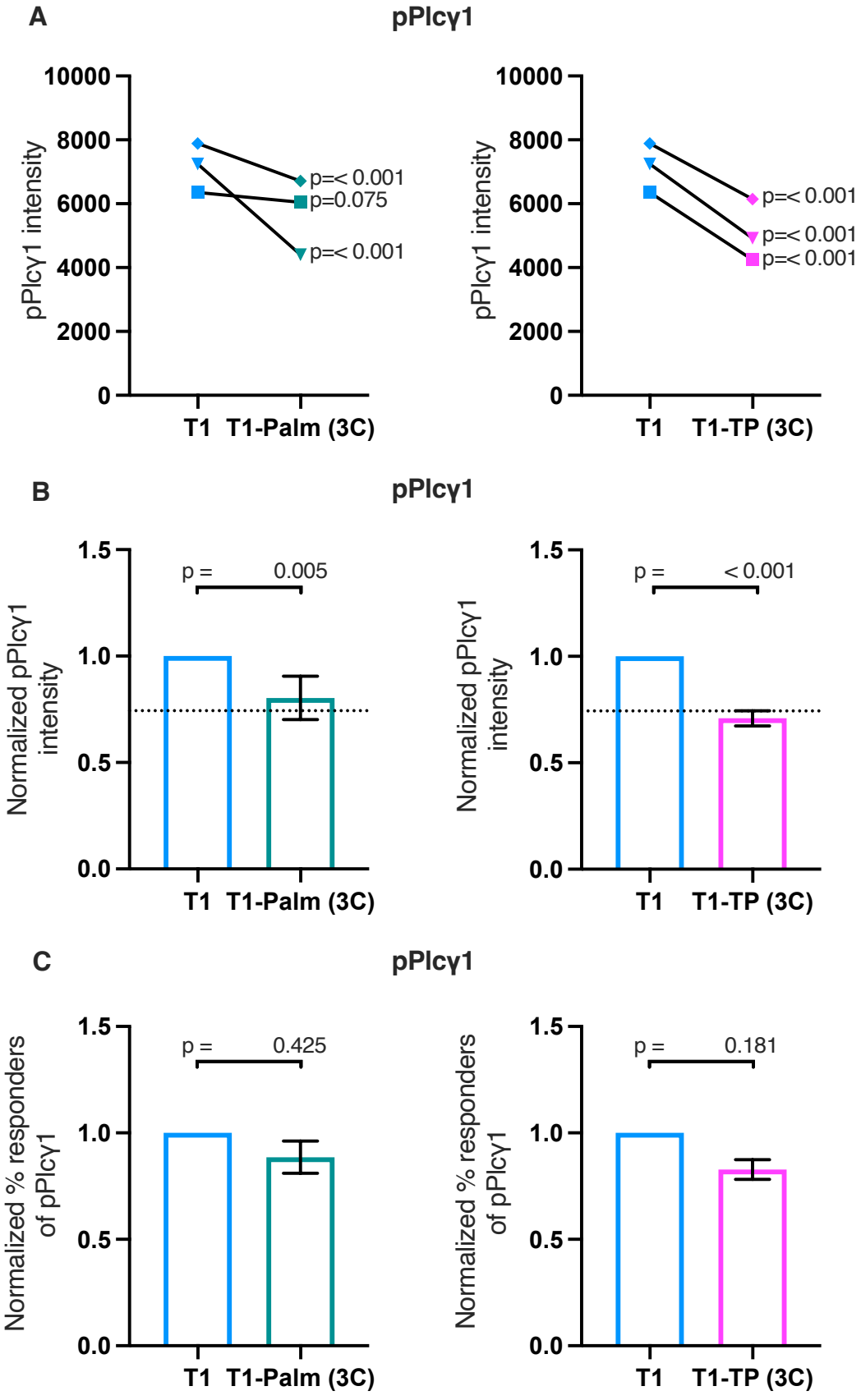

Figure 5 — figure supplement 2

Table 1. Motifs and mutants analyzed in this study.

Motif location/known function	Mutant Names	Mutated Motif	Residue Mutations
C-terminally truncated CD4	T1	Ends at R422	R422 is the last residue
Extracellular D1 C"-strand (binds pMHCII)	$T1^{\Delta bind}$	GKGVLIR	K68D, V70D, L71S, I72D, R73S
TMD/Protein or cholesterol interactions	T1-TMD	GGxxG	G403V, G406L
Juxtamembrane/Palmitoylation	T1-Palm (2C)	CV+C	C418S, C421S
Juxtamembrane/Palmitoylation	T1-Palm (3C)	CCV+C	C471S,C418S, C421S
TMD+Palm/raft localization	T1-TP (2C)	GGxxG, CV+C	G403V, G406L, C418S, C421S
TMD+Palm/raft localization	T1-TP (3C)	GGxxG, CCV+C	G403V, G406L, C417S, C418S, C421S

Table 2. All values presented as percent of WT control (truncation average/WT average x 100) for normalized values.

Mutant Names	IL-2 magnitude	IL-2 sensitivity	Normalized pCD3ζ intensity	Normalized % Responders pCD3ζ	Normalized pZap70 intensity	Normalized % Responders pZap70	Normalized pPlcγ1 intensity	Normalized % Responders pPlcγ1	Lck DRM AUC	Lck Total AUC	Lck DSM AUC	CD4 expression	CD4 endocytosis
WT	100	100	100	100	100	100	100	100	100	100	100	100	100
T1	61.46	13.52	106.30	95.20	106.10	102.20	104.40	112.60	28.81	19.22	16.08	110.09	14.30

Table 3. All values presented as percent of T1 control (mutant average/T1 average x 100) for normalized values.

Mutant Names	IL-2 magnitude	IL-2 sensitivity	Normalized pCD3ζ intensity	Normalized % Responders pCD3ζ	Normalized pZap70 intensity	Normalized % Responders pZap70	Normalized pPlcγ1 intensity	Normalized % Responders pPlcγ1	Lck DRM AUC	Lck Total AUC	Lck DSM AUC	CD4 expression	CD4 endocytosis
T1	100	100	100	100	100	100	100	100	100	100	100	100	100
T1$^{\Delta bind}$	1.53	0.00	54.86	91.39	71.96	111.9	74.32	106.8	ND	ND	ND	73.93	38.71
TMD	53.54	17.05	76.68	94.23	88.36	98.77	88.24	107.40	62.36	92.97	110.94	131.10	3.63
Palm (2C)	57.99	116.07	76.35	94.09	86.17	93.03	92.09	98.09	274.03	139.40	130.91	80.30	-98.00
TP (2C)	33.11	0.19	62.06	85.61	79.79	75.58	82.57	83.34	121.39	113.03	114.98	96.54	47.50
Palm (3C)	27.84	0.19	71.09	94.76	86.32	76.82	80.37	88.62	137.57	94.34	92.07	87.58	6.99
TP (3C)	31.19	45.53	62.49	84.60	80.16	66.92	70.91	82.81	86.84	101.20	102.74	79.59	-54.69

Figure Legends

Figure 1. Computational reconstruction of CD4 evolution.
The maximum likelihood phylogenetic tree clusters mammalian CD4 sequences. The tree highlights ancestral reconstructions of CD4 sequences from marsupials (kangaroo silhouette), Atlantogenata (elephant), and Boreoeutheria (wildcat). The logoplot of extant eutherian (Atlantogenata and Boreoeutheria) CD4 sequences show sequence conservation over evolutionary time. In these plots, the height of symbols indicates the relative frequency of each amino acid at that specific position. The mouse CD4 numbering (uniprot) is used as a reference, and residues are color-coded based on sidechain polarity. Evolutionary insertion or deletion events are indicated by dashes (-). Most recent common ancestor (MRCA) sequences are shown at each node in the tree (Node 1-4). As in our previous study (Lee et al., 2022), the ratio of synonymous (dS) and nonsynonymous (dN) substitution rates was calculated. Black dots indicate dN/dS ratios that are significantly below 1 across the entire dataset. Red dots indicate residues under purifying selection in the mammalian only dataset. Previously identified motifs are indicated by boxes, while the intracellular domain helix is shaded gray. The arrow at position 422 indicates where CD4 was truncated (CD4-T1), while TMD and T1-Palm show the mutations studied in this study.

Figure 2. Truncating CD4 does not reduce CD3ζ phosphorylation.
(**A**) Representative IL-2 production is shown in response to a titration of MCC peptide from one experiment (left). Experiments were performed in triplicate and each symbol equals the mean +/- SEM at that peptide concentration. AUC analysis for the dose response is shown as a measure of the response magnitude for the average of three independent experiments performed with one independently generated set of cell lines (center). The average response to a low dose (41nM) of peptide is shown as a measure of sensitivity for three independent experiments performed with one independently generated set of cell lines (right). The data are representative of those obtained with 4 (WT vs T1) or 2 (WT vs $T1^{\Delta bind}$) independently generated sets of cell lines.
(**B**) Phosphorylation intensity of CD3ζ (pCD3ζ) for WT and CD4-T1 (T1) (left), normalized pCD3ζ intensity for WT and T1 (center), and normalized % responders of pCD3ζ for WT and T1 (right). Five independently generated cell lines (biological replicates) were tested for WT and T1. For phosphorylation intensity, each pair of lines (connected symbols) was tested in three independent experiments. Data were analyzed and collected as in Figure 2 – figure supplement 3. One-way ANOVA was performed with a Dunnett's posttest using GraphPad Prism9. For normalized intensity and % responders, all individual mutant cell line values were normalized to their paired control values. Bars represent the mean +/- SEM. One-way ANOVA was performed with a Sidak's posttest for specific comparisons of normalized values using GraphPad Prism9.
(**C**) Phosphorylation intensity of pCD3ζ for T1 and $T1^{\Delta bind}$ (left), normalized pCD3ζ intensity for T1 and $T1^{\Delta bind}$ (center), and normalized % responders of pCD3ζ for T1 and $T1^{\Delta bind}$ (right) were performed and analyzed as in B, with the exception that the open symbols represent data from a single experiment whereas the closed symbols represent aggregate data from three independent experiments. Two-tailed t tests were performed

612 to compare the single T1 vs T1$^{\Delta bind}$ samples as no other samples were collected in
613 parallel.
614
615 **Figure 2- figure supplement 1.**
616 Flow cytometry analysis of CD4 (left) and TCR (right) expression on 58$\alpha^-\beta^-$ hybridoma
617 cells. Parental 58$\alpha^-\beta^-$ hybridoma cells served as negative control for surface expression
618 (open black histogram trace).
619
620 **Figure 2- figure supplement 2.**
621 TCR (left) and CD4 (right) endocytosis after pMHCII engagement is shown for the
622 indicated cell lines after 16 hours coculture with APCs in the presence of 10μM MCC
623 peptide. The change in TCR and CD4 gMFI, as measured by flow cytometry, is shown
624 for each cell line relative to an equivalent sample cultured with APCs in the absence of
625 MCC peptide. Each data point represents the mean ± SEM for three independent
626 experiments. For endocytosis measurements were performed in triplicate for each
627 experiment. One-way ANOVA was performed with a Dunnett's posttest.
628
629 **Figure 2-figure supplement 3.**
630 Example of intracellular signaling analysis workflow.
631 (**A**) Flow cytometry analysis of WT 58$\alpha^-\beta^-$ hybridoma:M12 cell couples. Representative
632 dot plots are shown for TCRβ^{GFP+} CD4$^+$ 58$\alpha^-\beta^-$ hybridoma cells coupled to Tag-it Violet-
633 labeled M12s expressing the indicated tethered pMCHII Hb:I-E^k (left) and MCC:I-E^k
634 (center). Representative histograms of WT 58$\alpha^-\beta^-$ hybridoma cells coupled to M12 cells
635 transduced to express the indicated tethered pMHCII are shown for pCD3ζ intensity
636 (right). 10,000 coupled cells were collected per individual experiment.
637 (**B**) Flow cytometry analysis of T1 58$\alpha^-\beta^-$ hybridoma-M12 cell couples. Representative
638 dot plots are shown for TCRβ^{GFP+} CD4$^+$ 58$\alpha^-\beta^-$ hybridoma cells coupled to Tag-it Violet-
639 labeled Hb:I-E^{k+} (left) and MCC:I-E^{k+} (center) M12 cells. Representative histograms of
640 T1 58$\alpha^-\beta^-$ hybridoma cells coupled to M12 cells expressing the indicated tethered
641 pMHCII are shown for pCD3ζ intensity (right). 10,000 coupled cells were collected per
642 individual experiment.
643 (**C**) A representative smoothed overlapping histogram of pCD3ζ intensity is shown for
644 58$\alpha^-\beta^-$ cells coupled to Hb:I-E^{k+} (cyan) or MCC:I-E^{k+} (black) M12 cells. Histogram of
645 pCD3ζ intensity for 58$\alpha^-\beta^-$ cells coupled to MCC:I-E^{k+} M12 cells subtracted from Hb:I-
646 E^{k+} M12 cell couples show the difference in pCD3ζ intensity on a bin-by-bin basis after
647 stimulation with agonist MCC:I-E^k compared with null Hb:I-E^k for WT (left) and T1
648 (center) cells. Overlapping pCD3ζ histogram (right) of cells responding to MCC:I-E^k
649 after Hb:I-E^k subtraction shows the responding populations for the WT and T1 cell lines.
650 Data represent the aggregate from three individual experiments (30,000 couples
651 analyzed). One-way ANOVA was performed with a Dunnett's posttest for comparison
652 with the WT sample because other mutants were simultaneously analyzed in this
653 experiment (not shown).
654 (**D**) Concatenated pCD3ζ average intensity ± SEM of WT and T1 cells (left) and the
655 percent of responding WT and T1 cells (right).
656

Figure 2-figure supplement 4.
(**A**) Zap70 (left), and Plcγ1 (right) phosphorylation intensity for WT and T1 are shown for paired (connecting line) WT and T1 cell lines. Five independently generated cell lines were tested (biological replicates). For phosphorylation intensity, each pair of lines (connected symbols) was tested in three independent experiments (technical replicates). The data from those experiments was aggregated, and the symbols represent the mean intensity of the aggregated pCD3ζ intensity values. One-way ANOVA was performed with a Dunnett's posttest.
(**B**) Average T1 phosphorylation for Zap70 (left) and Plcγ1 (right) from A are shown normalized to the paired WT controls. Bars represent the mean +/- SEM. One-way ANOVA was performed with a Sidak's posttest for specific comparisons.
(**C**) Average T1 % responders for pZap70 (left), and pPlcγ1 (right) are shown normalized to the paired WT controls for the cell lines shown in A. Bars represent the mean +/- SEM. One-way ANOVA was performed with a Sidak's posttest for specific comparisons.

Figure 2-figure supplement 5.
(**A**) Phosphorylation intensity for T1 and $T1^{\Delta bind}$ Zap70 (left), and Plcγ1 (right) are shown for paired (connecting line) T1 and $T1^{\Delta bind}$ cell lines. Three independently generated cell lines were tested (biological replicates). Analysis was performed as in Figure 2— figure supplement 4 with the exception that the open symbol represent data from a single experiment whereas the closed symbols represent the average of aggregated data from three independent experiments. For the open symbol comparisons we performed a two-tailed t test as no other samples were collected in parallel.
(**B**) Average $T1^{\Delta bind}$ cell line phosphorylation intensity for Zap70 (left), and Plcγ1 (right) are shown normalized to the average intensity of the paired T1 control cells shown in A. Analysis was performed as in Figure 2— figure supplement 4.
(**C**) Average $T1^{\Delta bind}$ cell line % responders for pZap70 (left) and pPlcγ1 (right) are shown normalized to their paired T1 control. Analysis was performed as in Figure 2— figure supplement 4.

Figure 3. The GGXXG and CV+C motifs are key determinants of CD4 function.
(**A, B**) Representative IL-2 production is shown in response to a titration of MCC peptide from one experiment (left). Experiments were performed in triplicate and each symbol equals the mean +/- SEM at that peptide concentration. AUC analysis for the dose response is shown as a measure of the response magnitude for the average of three independent experiments performed with one independently generated set of cell lines (center). The average response to a low dose (41nM) of peptide is shown as a measure of sensitivity for three independent experiments performed with one independently generated set of cell lines (right). Results are representative of those obtained with at least three independently generated sets of cell lines. One-way ANOVA was performed with a Dunnett's posttest for comparisons with WT and T1 samples, and a Sidak's posttest for comparisons between selected samples.

Figure 3- figure supplement 1.

(**A, B**) Flow cytometry analysis of CD4 (left) and TCR (right) expression on $58\alpha^-\beta^-$ hybridoma cells. Parental $58\alpha^-\beta^-$ hybridoma cells served as negative control for surface expression (open black histogram trace).

Figure 3- figure supplement 2.
(**A, B**) Lck signal is shown for each sucrose fraction normalized to the CD4 signal detected in the corresponding fraction (left). The AUC is shown for the normalized Lck signal in the DRM (center) and DSM (right) fractions. Each data point represents the mean +/- SEM for three independent experiments with the same cell line. Data are representative of experiments performed with three independently generated sets of lines for TMD, Palm(3C), and TP(3C) mutants. Analysis was performed with two set of lines for the Palm(2C) and TP(2C) mutants. One-way ANOVA was performed with a Dunnett's posttest for comparisons with WT and T1 samples, and a Sidak's posttest for comparisons between selected samples.

Figure 3- figure supplement 3.
(**A, B**) Total Lck signal (total AUC for sucrose gradient) normalized to CD4 signal is shown for the indicated cell lines. Each data point represents the mean +/- SEM for three independent experiments with the same cell line (experimental replicates). Data are representative of experiments performed with three independently generated sets of lines for TMD, Palm(3C), and TP(3C) mutants (biological replicates). Analysis was performed with two set of lines for the Palm(2C) and TP(2C) mutants. One-way ANOVA was performed with a Dunnett's posttest for comparisons with WT and T1 samples, and a Sidak's posttest for comparisons between selected samples.

Figure 3- figure supplement 4.
(**A, B**) TCR (left) and CD4 (right) endocytosis after pMHCII engagement is shown for the indicated cell lines after 16 hours coculture with APCs in the presence of 10μM MCC peptide. The change in TCR and CD4 gMFI, as measured by flow cytometry, is shown for each cell line relative to an equivalent sample cultured with APCs in the absence of MCC peptide. Each data point represents the mean ± SEM for three independent experiments (experimental replicates). Data are representative of those acquired with at least two independently generated sets of cell lines (biological replicates). Endocytosis measurements were performed in triplicate (technical replicates) for each experiment. One-way ANOVA was performed with a Dunnett's posttest for comparisons with WT and T1 samples.

Figure 4. The GGXXG and CV+C motifs reduce pCD3ζ levels.
(**A**) Phosphorylation intensity of CD3ζ for T1 and T1-TMD (left), T1 and T1-Palm (2C) (center), and T1 and T1-TP (2C) (right) are shown for independently generated pairs of (connecting line) T1 and T1-TMD (left), T1 and T1-Palm (2C) (center), and T1 and T1-TP (2C) (right) cell lines. Each pair of lines (connected closed symbols) was tested in three independent experiments (technical replicates). The data from those experiments was aggregated, and the symbols represent the mean intensity of the aggregated pCD3ζ intensity values. One-way ANOVA was performed with a Dunnett's posttest using GraphPad Prims 9.

(**B**) Data for each cell line in **A** are shown as the average pCD3ζ intensity for all T1-TMD (left), T1-Palm (2C) (center), and T1-TP (2C) (right) cell lines normalized to their paired T1 control. Dotted line is the normalized pCD3ζ intensity for $T1^{\Delta bind}$ as a visual reference point for the contributions of CD4-pMHCII interactions. Bars represent the mean +/- SEM. One-way ANOVA was performed with a Sidak's posttest for specific comparisons using GraphPad Prims 9.
(**C**) The average % responders for phosphorylation of CD3ζ is shown for T1-TMD (left), T1-Palm (2C) (center), and T1-TP (2C) (right) normalized to their paired T1 control line. Bars represent the mean +/- SEM. One-way ANOVA was performed with a Sidak's posttest for specific comparisons using GraphPad Prims 9.

Figure 4- figure supplement 1.
(**A**) Phosphorylation intensity of Zap70 for T1 and T1-TMD (left), T1 and T1-Palm (2C) (center), and T1 and T1-TP (2C) (right) are shown for paired (connecting line) cell lines. Analysis was performed as in Figure 4A.
(**B**) Normalized phosphorylation intensity of Zap70 for T1-TMD (left), T1-Palm (2C) (center), and T1-TP (2C) (right) are shown as bars. Analysis was performed as in Figure 4B.
(**C**) Normalized % responders of the phosphorylation Zap70 for T1-TMD (left), T1-Palm (2C) (center), and T1-TP (2C) (right) are shown as bars for T1 and $T1^{\Delta bind}$ cell lines. Analysis was performed as in Figure 4C.

Figure 4- figure supplement 2.
(**A**) Phosphorylation intensity of Plcγ1 for T1 and T1-TMD (left), T1 and T1-Palm (2C) (center), and T1 and T1-TP (2C) (right) are shown for paired (connecting line) cell lines. Analysis was performed as in Figure 4A.
(**B**) Normalized phosphorylation intensity of Plcγ1 for T1-TMD (left), T1-Palm (2C) (center), and T1-TP (2C) (right) are shown as bars. Analysis was performed as in Figure 4B.
(**C**) Normalized % responders of phosphorylated pPlcγ1 for T1-TMD (left), T1-Palm (2C) (center), and T1-TP (2C) (right) are shown as bars for T1 and $T1^{\Delta bind}$ cell lines. Analysis was performed as in Figure 4C.

Figure 4- figure supplement 3. Representative IL-2 production is shown in response to M12 cells transduced to express tethered MCC:I-E^k constructs as used in phosphorylation analysis. Experiments were performed in triplicate and each bar equals the mean +/- SEM at that peptide concentration. Results are representative of those obtained with two independently generated matched sets of cell lines. One-way ANOVA was performed with a Dunnett's posttest for comparisons with WT and T1 samples, and a Sidak's posttest for comparisons between selected samples.

Figure 5. The (C/F)CVRC motifs reduces proximal TCR-CD3 signaling.
(**A**) Phosphorylation intensity of CD3ζ for T1 and T1-Palm (3C) (left) and T1 and T1-TP (3C) (right) are shown for independently generated pairs of (connecting lines) T1 and T1-Palm (3C) (left) and T1 and T1-TP (3C) (right) cell lines. Analysis was performed as in Figure 4A.

(**B**) Data for each mutant cell line in **A** are shown as the average pCD3ζ intensity values for T1-Palm (3C) (left) and T1-TP (3C) (right) normalized to their paired T1 controls. The dotted line represents the normalized phosphorylation CD3ζ intensity for $T1^{\Delta bind}$ as a visual reference for the contributions of CD4-pMHCII interactions. Analysis was performed as in Figure 4C.
(**C**) Average % responders for phosphorylation of CD3ζ is shown for T1-Palm (3C) (left) and T1-TP (3C) (right) normalized to their paired T1 control. Analysis was performed as in Figure 4C.

Figure 5- figure supplement 1.
(**A**) Phosphorylation intensity of Zap70 for T1 and T1-Palm (3C) (left) and T1 and T1-TP (3C) (right) are shown for paired (connecting line) cell lines. Analysis was performed as in Figure 5A.
(**B**) Normalized phosphorylation intensity of Zap70 for T1-Palm (3C) (left) and T1-TP (3C) (right) are shown as bars. Analysis was performed as in Figure 5B.
(**C**) Normalized % responders of phosphorylated Zap70 for T1-Palm (3C) (left) and T1-TP (3C) (right) are shown as bars. Analysis was performed as in Figure 5C.

Figure 5- figure supplement 2.
(**A**) Phosphorylation intensity of Plcγ1 for T1 and T1-Palm (3C) (left) and T1 and T1-TP (3C) (right) are shown for paired (connecting line) cell lines. Analysis was performed as in Figure 5A.
(**B**) Normalized phosphorylation intensity of Plcγ1 for T1-Palm (3C) (left) and T1-TP (3C) (right) are shown as bars. Analysis was performed as in Figure 5B.
(**C**) Normalized % responders of phosphorylated Plcγ1 for T1-Palm (3C) (left) and T1-TP (3C) (right) are shown as bars. Analysis was performed as in Figure 5C.